END

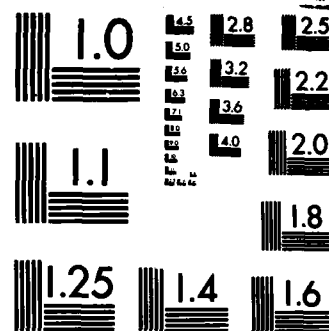MICROCOPY RESOLUTION TEST CHART

NATIONAL BUREAU OF STANDARDS-1963-A

AFWAL-TR-85-4010

Exploratory Development of FMR Advanced Surface Flaw Detection Methods

AD-A157 438

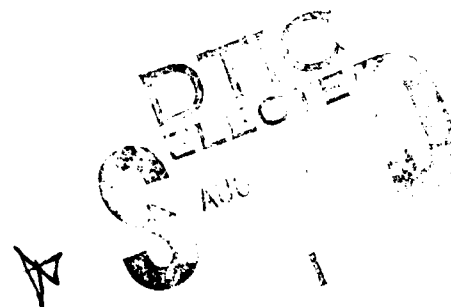Battelle, Pacific Northwest Laboratories
P.O. Box 999
Richland, Washington 99352

April 1985

Final Report for Period August 1982 - August 1984

APPROVED FOR PUBLIC RELEASE; DISTRIBUTION UNLIMITED

Materials Laboratory
Air Force Wright Aeronautical Laboratories
Air Force Systems Command
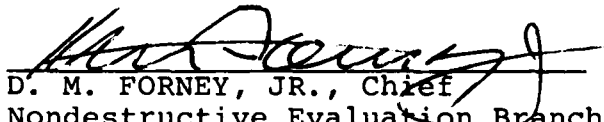Wright-Patterson Air Force Base, Ohio 45433

85 7 23 043

NOTICE

When Government drawings, specifications, or other data are used for any purpose other than in connection with a definitely related Government procurement operation, the United States Government thereby incurs no responsibility nor any obligation whatsoever; and the fact that the government may have formulated, furnished, or in any way supplied the said drawings, specifications, or other data, is not to be regarded by implication or otherwise as in any manner licensing the holder or any other person or corporation, or conveying any rights or permission to manufacture, use, or sell any patented invention that may in any way be related thereto.

This report has been reviewed by the Office of Public Affairs (ASD/PA) and is releasable to the National Technical Information Service (NTIS). At NTIS, it will be available to the general public, including foreign nations.

This technical report has been reviewed and is approved for publication.

JOSEPH A. MOYZIS, JR.
Nondestructive Evaluation Branch
Metals and Ceramics Division

FOR THE COMMANDER

D. M. FORNEY, JR., Chief
Nondestructive Evaluation Branch
Metals and Ceramics Division

"If your address has changed, if you wish to be removed from our mailing list, or if the addressee is no longer employed by your organization, please notify AFWAL/MLLP, W-PAFB, OH 45433 to help us maintain a current mailing list."

Copies of this report should not be returned unless return is required by security considerations, contractual obligations, or notice on a specific document.

REPORT DOCUMENTATION PAGE

1a. REPORT SECURITY CLASSIFICATION UNCLASSIFIED		1b. RESTRICTIVE MARKINGS			
2a. SECURITY CLASSIFICATION AUTHORITY		3. DISTRIBUTION/AVAILABILITY OF REPORT Approved for public release; distribution unlimited.			
2b. DECLASSIFICATION/DOWNGRADING SCHEDULE					
4. PERFORMING ORGANIZATION REPORT NUMBER(S)		5. MONITORING ORGANIZATION REPORT NUMBER(S) AFWAL-TR-85-4010			
6a. NAME OF PERFORMING ORGANIZATION Battelle, Pacific Northwest Laboratories	6b. OFFICE SYMBOL (If applicable)	7a. NAME OF MONITORING ORGANIZATION Materials Laboratory (AFWAL/MLLP) AF Wright Aeronautical Laboratories (AFSC)			
6c. ADDRESS (City, State and ZIP Code) Richland, Washington 99352		7b. ADDRESS (City, State and ZIP Code) Wright-Patterson Air Force Base OH 45433			
8a. NAME OF FUNDING/SPONSORING ORGANIZATION	8b. OFFICE SYMBOL (If applicable)	9. PROCUREMENT INSTRUMENT IDENTIFICATION NUMBER F33615-82-C-5100			
8c. ADDRESS (City, State and ZIP Code)		10. SOURCE OF FUNDING NOS.			
		PROGRAM ELEMENT NO.	PROJECT NO.	TASK NO.	WORK UNIT NO.
11. TITLE (Include Security Classification) Exploratory Development of FMR Advanced Surface Flaw Detection Methods (U)		62102F	2418	05	35

12. PERSONAL AUTHOR(S) Prince, James M.; Auld, Bert A.				
13a. TYPE OF REPORT Final Report	13b. TIME COVERED FROM 8/1/82 TO 8/1/84	14. DATE OF REPORT (Yr., Mo., Day) 1985, April	15. PAGE COUNT 69	
16. SUPPLEMENTARY NOTATION				

17.	COSATI CODES		18. SUBJECT TERMS (Continue on reverse if necessary and identify by block number)
FIELD	GROUP	SUB. GR.	Nondestructive inspection; eddy-current; ferromagnetic resonance
14	0	2	
11	0	6	

19. ABSTRACT (Continue on reverse if necessary and identify by block number)

The purpose of this program was to carry forward the development of a microwave eddy current (MEC) probe, which is based on the ferromagnetic resonance (FMR) principle, to the point where its performance in a practical flaw detection breadboard system for gas turbine engine component inspection and its compatibility with the Retirement-for-Cause (RFC) modular inspection system could be demonstrated.

This program studied the physical constraints related to the inspection of complex geometries in Ti 6-2-4-6 and IN-100 materials with the MEC-FMR surface flaw detection method. Based on the resulting information, a breadboard inspection system was designed and fabricated to demonstrate the MEC-FMR test method in the inspection of a jet engine interstage seal key slot.

20. DISTRIBUTION/AVAILABILITY OF ABSTRACT UNCLASSIFIED/UNLIMITED ☒ SAME AS RPT. ☐ DTIC USERS ☐	21. ABSTRACT SECURITY CLASSIFICATION UNCLASSIFIED	
22a. NAME OF RESPONSIBLE INDIVIDUAL Joseph A. Moyzis, Jr.	22b. TELEPHONE NUMBER (Include Area Code) (513) 255-5309	22c. OFFICE SYMBOL AFWAL/MLLP

DD FORM 1473, 83 APR   EDITION OF 1 JAN 73 IS OBSOLETE.   UNCLASSIFIED

FOREWORD

This final technical report covers work performed under Contract F33615-82-C-5100 from 1 August 1982 to 31 July 1984. The work was administered under the technical direction of Mr. Charles Elias and Dr. Joseph Moyzis, Material Laboratory, Air Force Wright Aeronautical Laboratories, Wright-Patterson Air Force Base, Ohio 45433.

The contractor was the Nondestructive Testing Section of Battelle, Pacific Northwest Laboratories, Richland, Washington 99352. The principal investigator was Mr. Jim Prince. Other investigators were J. Mike King and Mike Dodson. The theoretical analysis was performed at Stanford University by Prof. Bert Auld.

iii

A-1

TABLE OF CONTENTS

LIST OF ILLUSTRATIONS

LIST OF ILLUSTRATIONS (cont'd)

LIST OF ILLUSTRATIONS (concluded)

ix

1.0 INTRODUCTION

This report describes the work performed by Battelle, Pacific Northwest Laboratories and Stanford University under Contract F33615-82-C-5100 with the Air Force Wright Aeronautical Laboratories. The project was specifically directed at developing a breadboard surface flaw detection system for the detection of fatigue cracks in complex geometry engine components made of Ti 6-2-4-6 or IN-100. In the project's first task, theoretical and experimental work were performed to characterize the FMR-MEC probe's surface flaw detection sensitivity as a function of probe liftoff, specimen material (Ti 6-2-4-6 and IN-100), specimen geometries in the area of the flaw and flaw length, depth and closure. The FMR-MEC probe design has been optimized in the single probe configuration for maximum flaw detection sensitivity on the flaw, material and geometry combination that pertains to a critical location in the engine component. The theoretical analysis and modeling was provided by Stanford University under subcontract to Battelle to help guide and analyze the Task I laboratory studies.

In the second task, Battelle designed and assembled a breadboard MEC flaw detection system to inspect the key slot geometry on a jet engine interstage seal component that was supplied by the Air Force. The system design is based on the information generated in Task I. Experiments were performed evaluating the breadboard system's sensitivity of detection on the key slot specimen as well as the specimens prepared in Task I. This evaluation provides information to assess the potential for inclusion of an FMR-MEC system based on the breadboard into the RFC modular inspection system.

In the third task, Battelle demonstrated the research results to the Air Force staff at AFWAL. The demonstration verified the breadboard system's practical performance and capabilities.

The microwave eddy current technology utilized in this project is based on the FMR characteristics of a GaYIG (Gallium-doped Yttrium Iron Garnet) sphere. When the GaYIG sphere is coupled to an excitation current source with a single turn loop of wire and immersed in a DC magnetic field, which is oriented approximately parallel with the loop plane, a magnetic precession occurs in the resonator material. With the resonating sphere placed close enough to a conductive material so that the precessing field links with the material, eddy currents are induced into the material. The eddy current field covers a surface area approximately corresponding to the diameter of the coupling loop, which is typically 0.1 millimeters larger in

1

diameter than the YIG sphere. The resultant surface and near-surface eddy currents in turn generate magnetic fields that link back to the resonating sphere affecting its characteristics, specifically the resonant frequency and Q. The diameter of the GaYIG sphere typically ranges from 0.25 to 0.75 millimeters, which accounts for its inherent high spatial resolution.

The approach followed by Battelle is to utilize the FMR probe in an active mode in which it operates as the resonant element of a microwave oscillator circuit (active FMR probe) at frequencies ranging from 600-1100 MHz. In this active mode, the excitation current is supplied by the oscillator circuitry at a frequency automatically set to the resonant frequency of the FMR probe.

Section 2.0 of this report discusses the experimental evaluation performed by Battelle, and Section 3.0 discusses the theoretical analysis and modelling performed by Stanford. Section 4.0 summarizes the work performed in this study and provides our conclusions.

2.0 EXPERIMENTAL EVALUATION

2.1 DETERMINE PHYSICAL CONSTRAINTS ON TEST METHOD (TASK I)

2.1.1 Electronically Modeling the Passive FMR Probe

In order to optimize the capabilities of the active FMR probe, it was necessary to electronically model the probe and gain an understanding of the relationship between its model components and its environment. The equivalent circuit model of the FMR probe is shown in Figure 1.
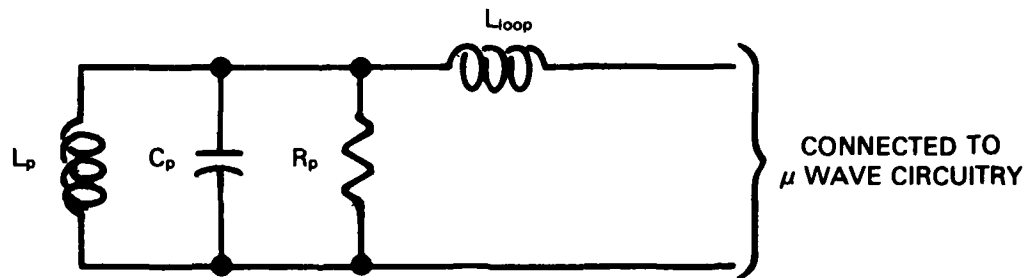
Figure 1.   FMR Probe Equivalent Circuit.

The FMR probe is electronically analyzed by plotting its reflection coefficient as a function of frequency on the Smith chart. This is accomplished with the set up shown in Figure 2. The test equipment shown here is an HP8754A and 8748A test set configured for measuring circuit reflection coefficients and transistor S-parameters over a frequency range of 4-2600 MHz.

FMR PROBE TEST FIXTURE   NETWORK ANALYZER AND S-PARAMETER
                                              TEST SET
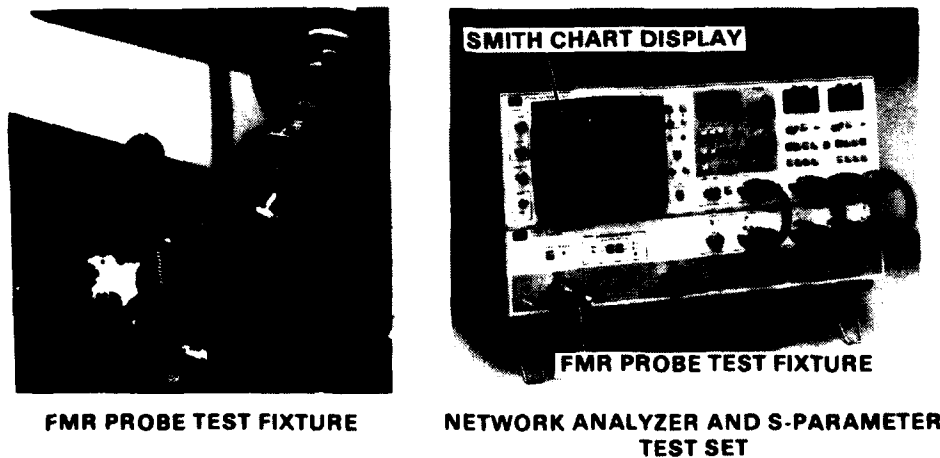
Figure 2.   Reflection Coefficient Measurement Set Up.

The FMR probe test fixture provides a method for studying the probe's electronic behavior as a function of its environment.

The component values for the FMR probe equivalent circuit (Figure 1) are resolved by fitting the results of the equivalent circuit impedance equation shown below with the Smith chart plot.

$$z = \frac{R_p(X_{c_p}X_{1_p})^2}{R_p{}^2(X_{c_p}-X_{1_p})^2+(X_{c_p}X_{1_p})^2} + j\left[\frac{R^2{}_p(X_{c_p}X_{1_p})(X_{c_p}-X_{1_p})}{R^2{}_p(X_{c_p}-X_{1_p})^2+(X_{c_p}X_{1_p})^2} + X_{L_{1oop}}\right].$$

Two FMR probe Smith chart plots are shown in Figure 3.
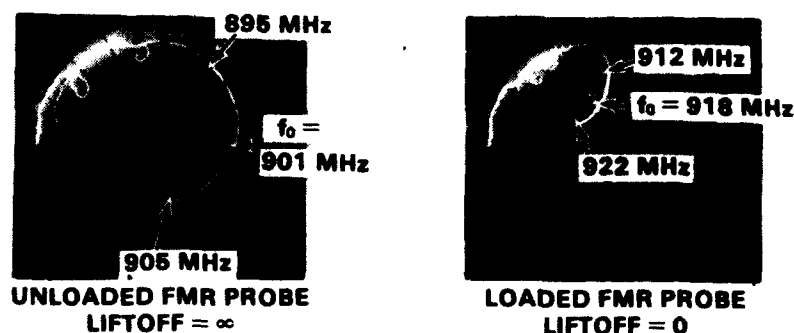
Figure 3. Typical FMR Probe Reflection Coefficient Plots.

The following equivalent circuit component values matched the calculated impedance with the respective Smith charts at the frequencies shown.

Unloaded FMR Probe (Liftoff = ∞)

L_p = 0.136 nh (nanohenry)
C_p = 230 pf (picofarad)
R_p = 175 ohms
L_{1oop} = 4.6 nh
Probe Q = 228

Loaded FMR Probe (Liftoff = 0)

L_p = 0.104 nh
C_p = 290 pf
R_p = 34 ohms
L_{1oop} = 4.6 nh
Probe Q = 57

4

Note the large change in R_p. We feel that this type of analysis will lead to an active probe design that will provide for flaw/liftoff separation in physically small probe designs.

Approximate values for the parallel components in the equivalent circuit can also be calculated for the unloaded FMR probe, as follows, when the physical parameters of the probe are known.[1,2]

$$Q_u = \frac{H_o - 1/3(4\pi M_s)}{\Delta H}$$

$$R_p = \mu_o \frac{V}{d_e^2} Q_u \, (2\pi\gamma)(4\pi M_s)$$

$$C_p = \frac{Q_u}{R_p \omega_o}$$

$$L_p = \frac{R_p}{Q_u \omega_o}$$

where:
Q_u = unloaded Q (liftoff = ∞)
H_o = f_o/γ, gauss
γ = 2.8 x 10^6 Hz/gauss, gyromagnetic ratio
$4\pi M_s$ = saturation magnetization of GaYIG, gauss
ΔH = line width of GaYIG, oersted
V = volume of GaYIG sphere, meter^3
d_e = effective diameter of loop, meter
μ_o = 4π x 10^{-7} henry/meter.

The key to the accuracy of these equations lies in the determination of the effective diameter of the loop. Using the measured loop diameter of 1 mm and the GaYIG manufacturer's specifications of V = 2.09 x 10^{-10} meter^3, $4\pi M_s$ = 250 gauss, and ΔH = 1 oersted, we calculate

Q_u = 238
L_p = 0.204 nh
C_p = 153 pf
R_p = 275 ohms

The results indicate that Q_u is very close to the measured value, but that the parallel component values differ from the measured values substantially indicating that the effective loop diameter does not equal the measured diameter of 1 mm. By adjusting the effective loop diameter to 1.25 mm and recalculating the parallel component values, we get much better results:

$$L_p = 0.131 \text{ nh}$$
$$C_p = 239 \text{ pf}$$
$$R_p = 176 \text{ ohms}$$

These calculated values serve nicely as initial values for the Smith chart impedance fitting process discussed earlier.

2.1.2 Characterization of FMR Probe in the Passive Mode

2.1.2.1 YIG Sphere Orientation Method for Mounting

One of the requirements for achieving repeatable FMR probe operation is that the crystallo-graphic orientation of the YIG sphere must be known when it is fixed to the YIG mounting rod. The YIG sphere is made from a cubic crystal material having a strong magneto-crystalline anisotropy. It has hard [100, etc.] axes of magnetization perpendicular to its cube faces and easy [111, etc.] axes of magnetization along its cube diagonal directions. One effect of this anisotropy is that the effective strength of the applied magnetic field on the YIG sphere changes with its orientation in the external DC magnetic field. This effect has been measured by observing the resonant frequency of an FMR probe with the YIG mounted with an easy axis perpendicular to the mounting rod. The mounting rod was then rotated with its axis perpendicular to the lines of the external DC magnetic field. The net effect was that the resonant frequency varied from 700 to 960 MHz, which corresponds to a change in the effective applied magnetic field on the YIG sphere of 93 gauss. This 30% change in the applied field strength signifies the importance of a repeatable YIG-sphere mounting procedure.

The easy axes can readily be located since the YIG sphere, when allowed to roll freely, will self orient an easy axis along the field direction of an external DC magnetic source. As shown in Figure 4, the easy axes can be marked by placing a spot of RTV on the top of the sphere as it rests on or near the surface of a permanent magnet. The other easy axes can be located by nudging the sphere off of the marked axis and on to another. By marking at least two adjacent easy axes, a hard axis can be located. However, if four adjacent axes are located and marked, final positioning of the sphere on the mounting rod is made much easier. In this case, the rod is cemented to the sphere with its axis in the center of the easy axis marks and thus on a hard axis. A fixture holds the rod at an angle of 35.3° above the permanent magnet face plane to assure the proper contact angle.

6
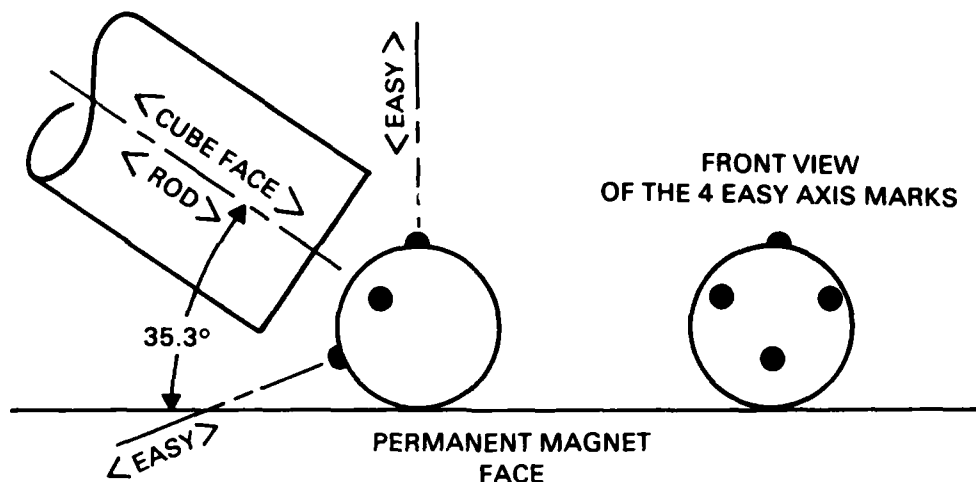
Figure 4. Easy and Cube Face Axes Location Method.

2.1.2.2 FMR Probe Temperature Stability Versus Orientation

The location of a hard axis is particularly important in performing experiments concerning temperature stability of the YIG FMR probe. It is well known in the YIG device industry that crystallo-graphic orientations in the external magnetic field exist that greatly suppress the affect of temperature on FMR probe resonance. This is an important factor in terms of absolute FMR-MRC probe engineering. For pure YIG material (we are using gallium-doped material in this work), optimum temperature independence should occur when the sphere is oriented so a hard axis is approximately 30° from the direction of the external field. Therefore, all possible external field directions that would satisfy this orientation form a 30° cone about each hard axis since all hard axes are equivalent.

The signals shown in Figure 5 are the result of setting up a pulsating heat source directed at a YIG sphere in an FMR probe test fixture. The signals were taken from the HP8754 network analyzer and represent approximately 20 MHz/volt shift in the probe resonant frequency. For the worst-case signals, this translates to a peak-to-peak frequency shift of 2.5 MHz. The optimum orientation allowed a 140 kHz shift for the same delta temperature. This is a 25 dB improvement in the reduction of unwanted temperature effects. At the optimum orientation one of the hard axes was approximately 30° from the direction of the external DC magnetic field. However, the magnitude of the temperature effects remained sensitive to the rotation of the probe on its mounting rod axis.

7

WORST-CASE   OPTIMUM-CASE
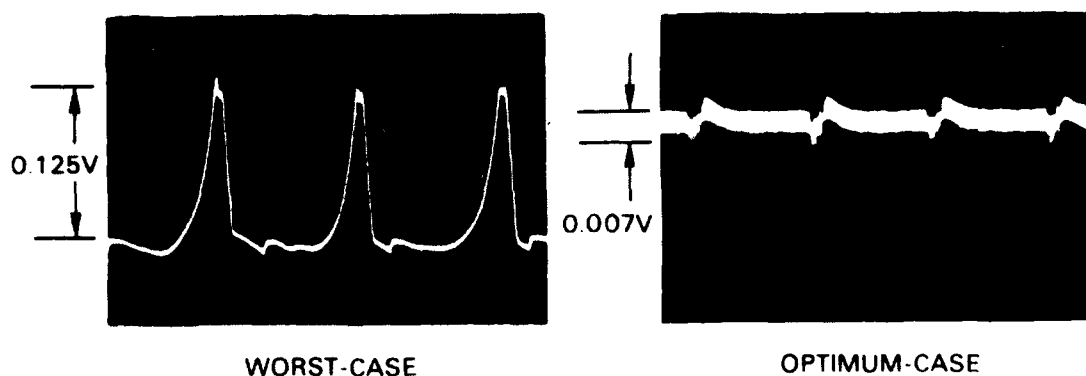
Figure 5. FMR Probe Temperature Response.

This implies that the hard axis did not exactly line up with
the probe mounting rod axis causing the field direction to rotate
out of the 30° cone about the hard axis. It was not determined
whether adequate flaw sensitivity can be maintained with the
FMR-MRC probe oriented for optimum temperature independence,
since sensitivity to flaws is also a function of probe/external
field orientation.

2.1.2.3 Flaw/Liftoff Separation in Reflection Coefficient Data

As a result of the theoretical analysis and modeling work
being performed at Stanford for this project, we have pursued the
philosophy   that if flaw/liftoff   discrimination could be
achieved in a practical single FMR-MEC probe configuration,
going to a dual-differential configuration would not be neces-
sary. Another factor is that the dual probe's size and com-
plexity may rule it out for certain tight geometry applications.

The reflection coefficient plot shown in the upper portion
of Figure 6 was taken with the microwave network analyzer con-
nected to a passive FMR probe. A titanium test specimen with a
0.63 mm long EDM notch in it was positioned approximately 0.13
mm from the probe. The liftoff and flaw loci were generated at
a fixed drive frequency of 750 MHz. The resonance loop was
generated by sweeping the drive about 750 MHz. It is clear from
these data that the FMR probe does provide a phase angle between
liftoff and flaw. The plot shown in the lower portion of Figure
6 illustrates the flaw/liftoff loci as a function of the location
of the drive frequency on the resonance loop. Utilizing these
data to equate flaw and liftoff responses to the equivalent
circuit model of the FMR probe, it should be possible to optimize
the active probe oscillator circuit for flaw/liftoff phase
separation.

8
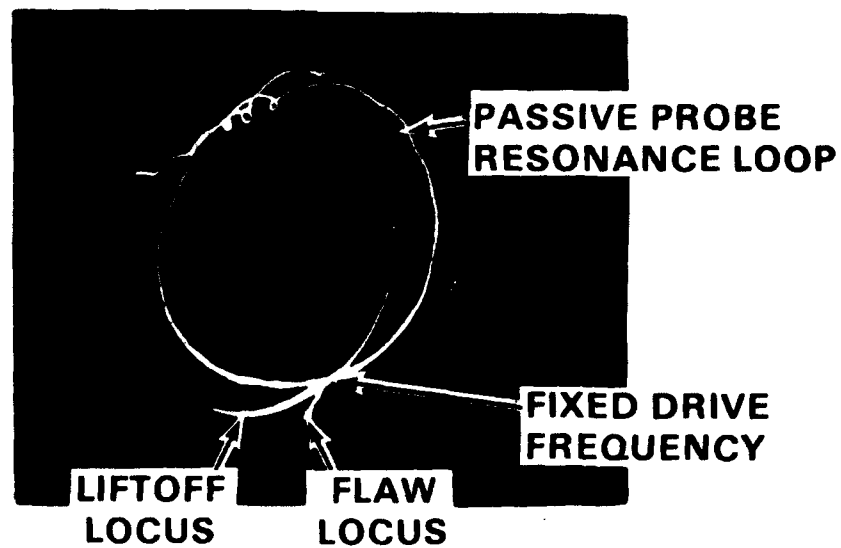
LIFTOFF AND FLAW RESPONSES ON REFLECTION COEFFICIENT PLOT
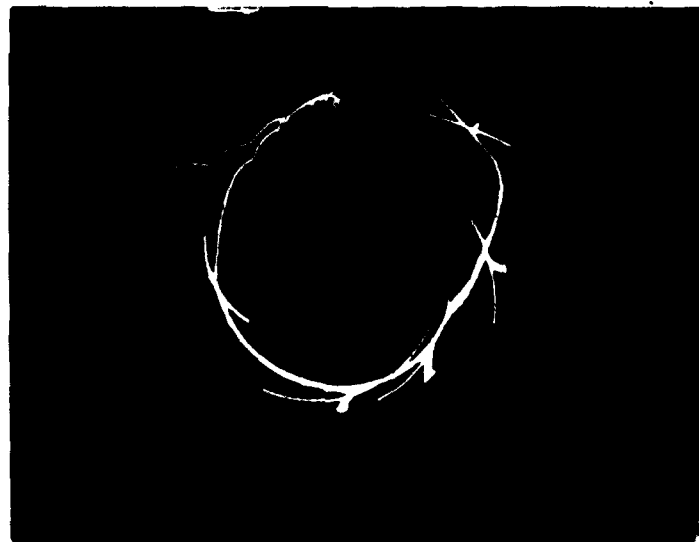
RESPONSES AT DIFFERENT DRIVE FREQUENCIES

Figure 6.   Flaw/Liftoff Separation on Passive FMR Probe.

2.1.2.4 FMR Probe Effective RF Field Plot

It is important to know what the shape of the FMR probe RF field is, particularly in applications where inspection is required in tight areas such as sharp inside corners. Knowing the RF field shape as a function of the FMR probe geometry allows the coupling loop and YIG sphere diameters to be chosen accurately for the specific inspection geometry.

The RF field test set up is shown in Figure 7 along with probe response curves taken with the network analyzer and a plot of data taken from these curves. A passive probe was connected to the network analyzer with a 0.38 mm diameter copper wire placed near the probe, as shown in the test set up, on an x-y positioner. The vertical and horizontal network analyzer outputs were connected to a storage scope to allow superimposing the curves onto one photograph. Each curve shows how the reflection coefficient of the FMR probe responded when the wire position was moved from outside the RF field (X greater than 1 mm) to directly in front of the probe (X = 0) at a given liftoff (Y). The scope horizontal position was adjusted manually to mark each curve at various X values and to spread out the curves along the horizontal axis. A plot of the relative probe responses versus the X displacement, shown at the bottom of Figure 7, indicates that the FMR probe RF field is confined and directed by the coupling loop. This conclusion was substantiated by observing that negligible response occurred when a copper strip was placed along side of the coupling loop in the same direction as the wire shown in the setup.

2.1.3 Development of FMR-MEC Signal Processing Methods

2.1.3.1 Flaw/Liftoff Separation from Active Probe Output Signal

As discussed earlier in this report, we were able to obtain flaw/liftoff separation in the reflection coefficient domain. This means that the electrcial complex impedance of the FMR probe changes in one manner for flaws and another for liftoff fluxuations. These changes can also be expressed in terms of resonator Q and resonant frequency. The active probe, which consists of an FMR probe (the resonator) in a transistor oscillator circuit, transforms these changes into its output in the form of amplitude and frequency. In order to evaluate the results of this transformation, we designed and fabricated the amplitude/frequency (A/F) signal processor shown in block diagram form in Figure 8. Actually, we fabricated a dual signal processor to facilitate testing of the dual-differential FMR probe as required. The A/F signal processor first converts the ultra-high frequency of the active probe output down to an intermediate frequency (IF) of approximately 50 MHz through a

10
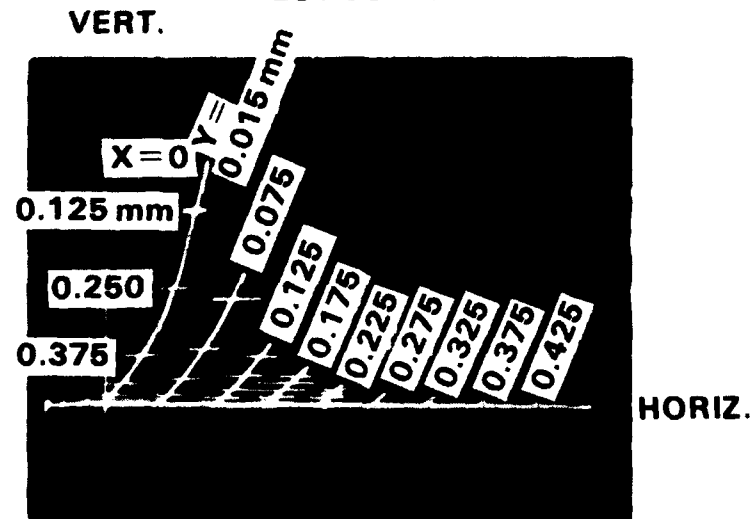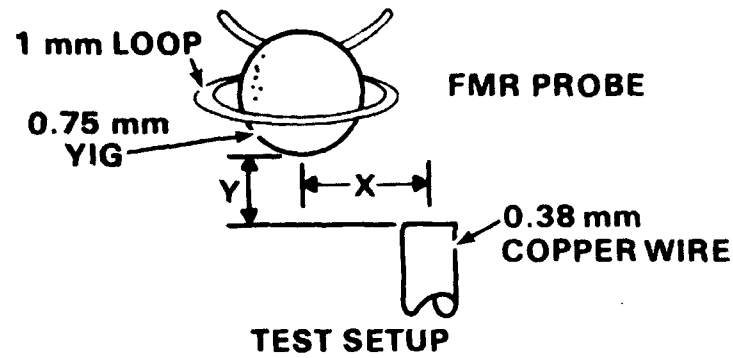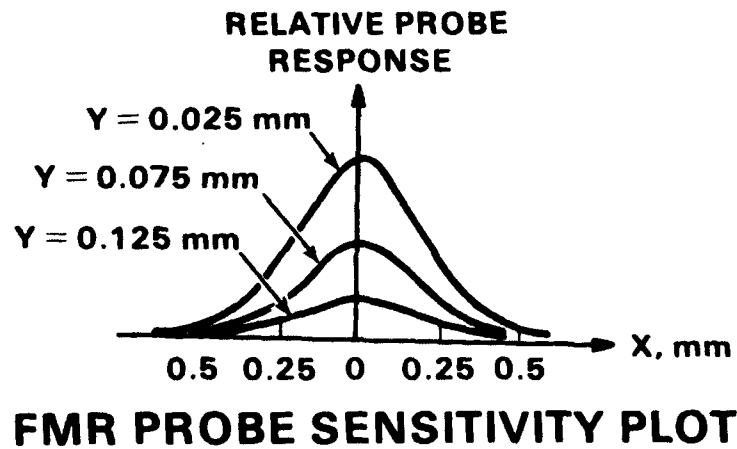
Figure 7. FMR Probe RF Field Test.

```
    VARACTOR
     TUNED
   OSCILLATOR

        AMPLIFIER
PROBE
OUTPUT─→(R  I)──→ ▷ ──┬──→ AMPLITUDE ──→ AMPL
( 870 MHz)              │     DETECTOR

   DOUBLE-BALANCED
       MIXER
                       │      LIMIT
                       └──→    AND     ──→ FREQ
                            FREQUENCY
                             DETECTOR
```

AMPLITUDE/FREQUENCY SIGNAL   FLAW 0.25 x 0.125 mm
          PROCESSOR   EDM NOTCH IN TITANIUM
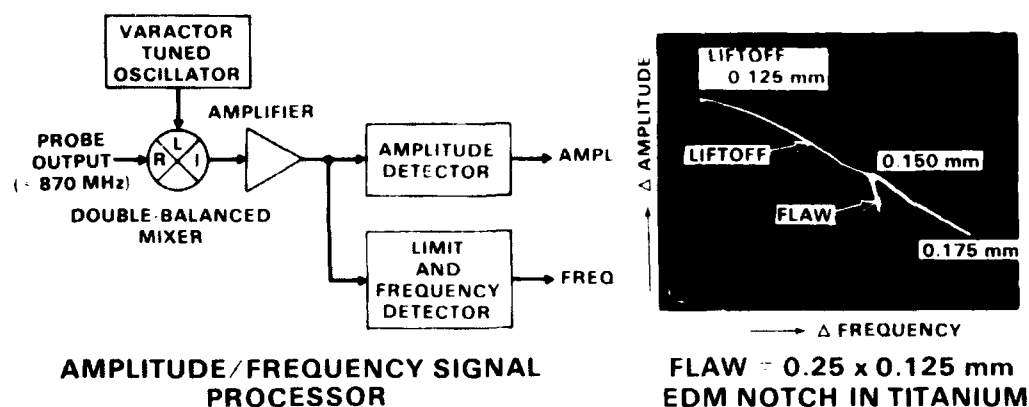
Figure 8.   Amplitude/Frequency Signal Processor with Flaw
            and Liftoff Response.

double-balanced mixer which preserves the amplitude information
in the probe output. The IF signal is then amplified and
presented to the amplitude and frequency detectors. The ampli-
tude detector is simply a peak follower. The frequency detector
first limits the IF signal to remove amplitude information. Then
it frequency demodulates the limited signal with one slope of a
bandpass filter and a peak detector. The data shown in Figure
8 was taken with a demonstration probe developed in a previous
contract.[3] The YIG sphere orientation was adjusted slightly
for optimum flaw/liftoff separation. The flaw response is from
a 0.25 mm by 0.13 mm EDM notch in a Ti 6-4 disk specimen with
liftoff set at 0.15 mm. Again, as with the passive probe
flaw/liftoff data (Figure 6), we see excellent phase separation
between the flaw response and the liftoff response.

In order to study this separation further in terms of
liftoff signal suppression, we designed and fabricated a signal
mixer. The mixer, which can mix up to four signals, will
accommodate dual-probe data mixing. The results of mixing
amplitude and frequency data from a single active probe are shown
in Figure 9. The numbers above each flaw signal identify which
EDM notch on a Ti 6-4 disk the flaw response is from. The disk
was shimmed to provide a 0.025 mm liftoff fluxuation. The
liftoff effects are clearly visible going into the mixer, which
was adjusted for optimum liftoff signal suppression at its
output as shown. The notch geometry and dimensional information
for the Ti 6-4 disk is shown in Figure 10.

DATA FROM TITANIUM DISK
Δ LIFTOFF = 0.025 mm

MIXED DATA FOR LIFTOFF
SIGNAL SUPPRESSION
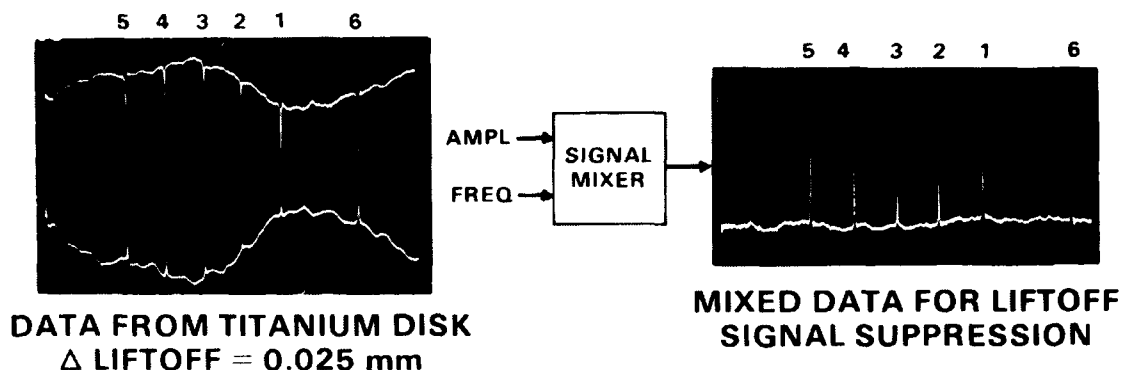
Figure 9.   Signal Mixer for Suppression of Liftoff Signal.

	L	W	D	mm (inch)
6	0.48 (0.019)	0.30 (0.012)	0.25 (0.010)	
5	0.43 (0.017)	0.14 (0.006)	0.25 (0.010)	
4	0.42 (0.017)	0.14 (0.006)	0.13 (0.005)	
3	0.24 (0.010)	0.13 (0.005)	0.25 (0.010)	
2	0.22 (0.009)	0.12 (0.005)	0.13 (0.005)	
1	0.36 (0.014)	0.36 (0.014)	0.25 (0.010)	

EDM NOTCH DIMENSIONS

NOTCH GEOMETRY FOR
Ti 6-4 DISK
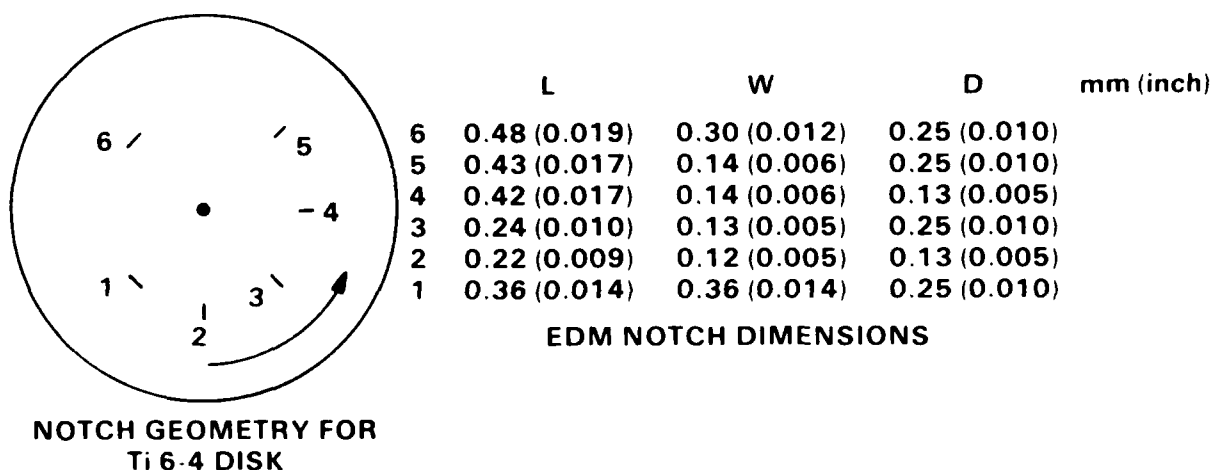
Figure 10.   Ti 6-4 Disk Geometry and Dimensions.

2.1.3.2   Mixed Data on IN-100 and Ti 6-2-4-6 Specimens

Experiments were performed on disk specimens of IN-100 and Ti 6-2-4-6 to evaluate the FMR-MEC method sensitivity as a function of these materials. A disk of each material was EDM notched as shown in Figure 11. The mixed data in this figure have been set for maximum liftoff suppression. Note that the reference notch response (EDM Notch #1) on both materials is approximately the same magnitude, indicating that the FMR-MEC method performs equally well on both materials. It can also be observed that some of the other notch responses are not equivalent from material to material. The reason for this is that even though the notch dimensions are extremely close on both disks, they were not put exactly on the same radius with respect to each other on either disk. Therefore, the probe must be positioned for maximum flaw response over the EDM notch of interest (Notch #1 for these data) which may tend to weaken the responses to other notches.

13

LENGTH | WIDTH | DEPTHS | mm (inch)

	LENGTH	WIDTH	DEPTHS	mm (inch)
5	0.50 (0.020)	0.13 (0.005)	GREATER THAN	
4	0.38 (0.015)	0.13 (0.005)	0.13 (0.005)	
3	0.38 (0.015)	0.13 (0.005)		
2	0.30 (0.012)	0.13 (0.005)		
1	0.30 (0.012)	0.13 (0.005)		

EDM NOTCH DIMENSIONS

**NOTCH GEOMETRY ON
IN-100 AND
Ti 6-2-4-6 DISKS**

2 1 5 4 3

0.30 mm LONG
MIXED DATA ON
IN-100 DISK

4 3 2 1 5

0.30 mm LONG
MIXED DATA ON
Ti 6-2-4-6
DISK
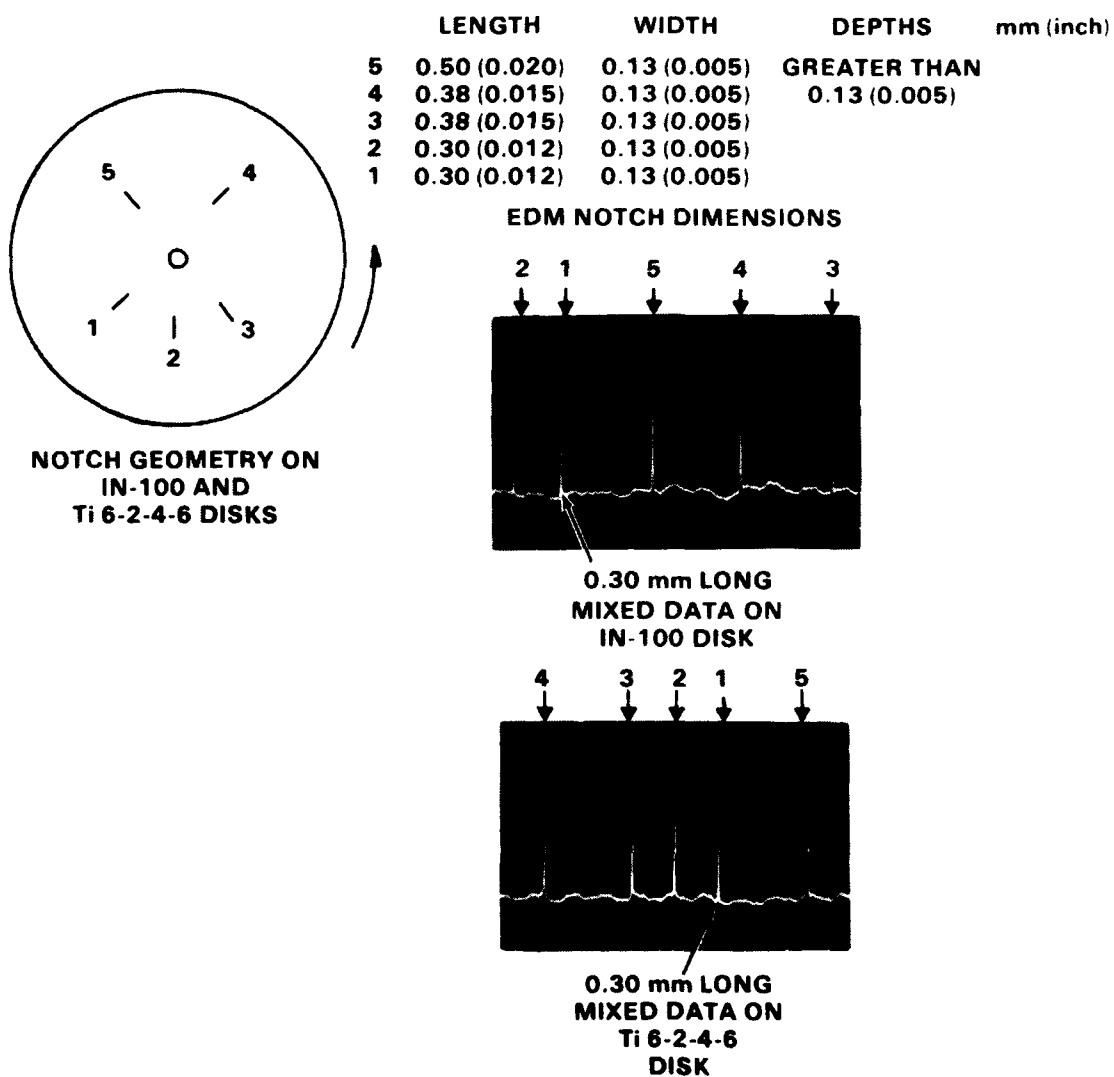
Figure 11.   EDM Notch Data on IN-100 and Ti 6-2-4-6.

14
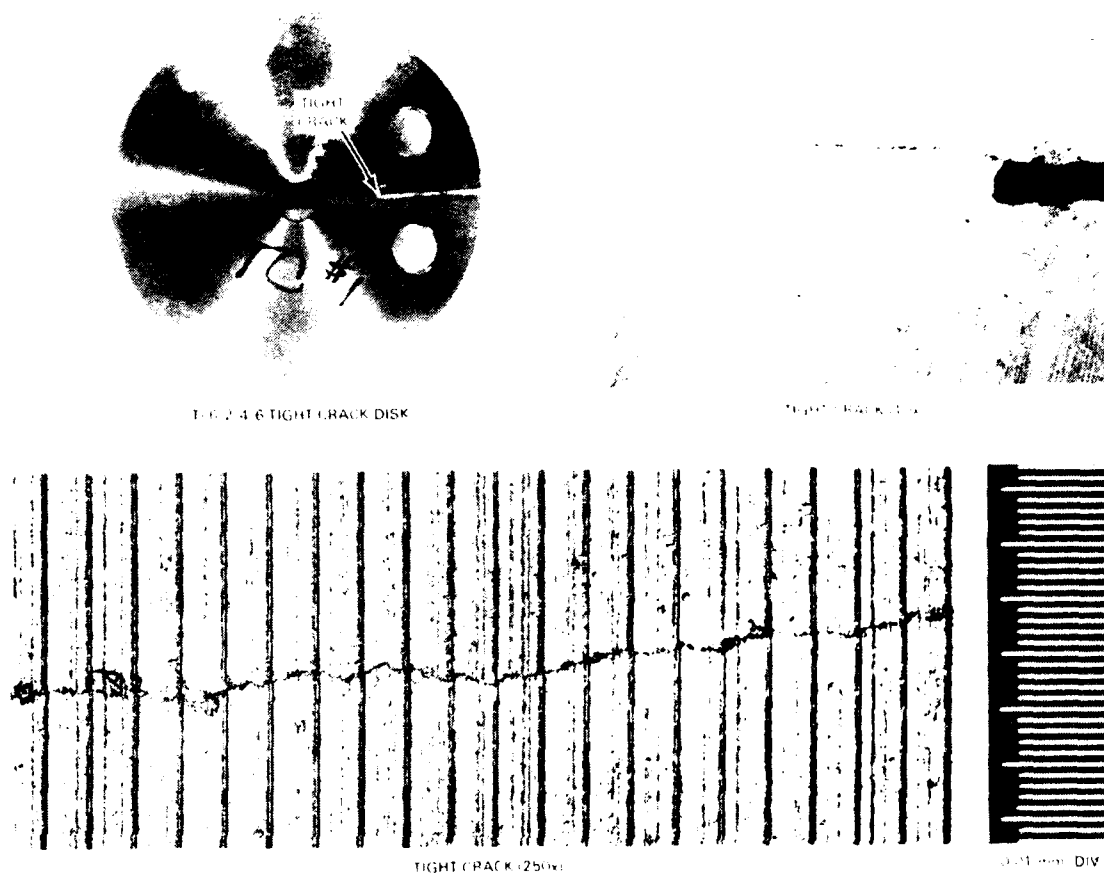
Figure 12. Tight Crack Disk Specimen.

The tight crack specimen shown in Figure 12 was fabricated on a Ti 6-2-4-6 disk. As shown, the crack width is in the order of 1-3 microns. The other marks running across the crack are machine marks still present on the unpolished disk from its being cut into the disk shape. These circular marks do not affect our test since we are scanning the surface in the same direction; i.e., approximately perpendicular to the crack on a fixed radius.

The mixed data on this tight crack is shown in the left photograph of Figure 13. The photograph on the right is data taken on the Ti 6-4 disk with the same probe, probe liftoff, and signal processor gain settings. By comparing response magnitudes, we see that this tight crack produces approximately the same response as the number 4 response on the disk which is from a 0.42 mm by 0.14 mm EDM notch (refer to Figure 10 for other Ti 6-4 disk notch dimensions). Considering that the effective

15

MIXED DATA ON
Ti 6-2-4-6
TIGHT CRACK DISK

MIXED DATA ON
Ti 6-4 DISK
WITH SAME GAIN
AND LIFTOFF SETTINGS
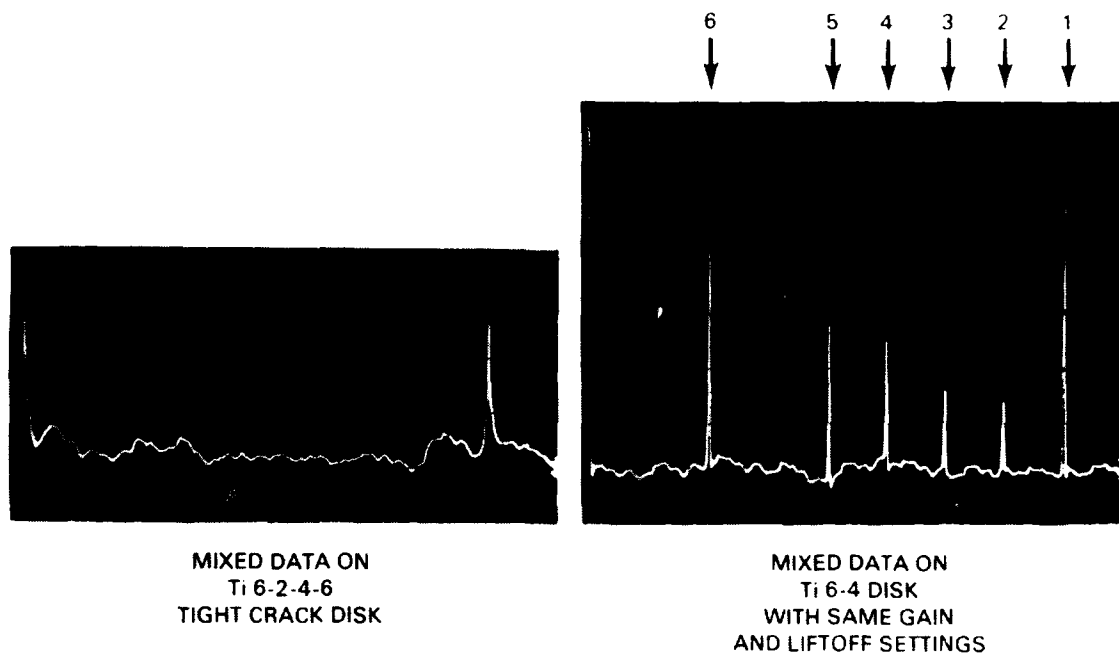
Figure 13. Tight Crack Data on Disk Specimen.

sensitivity of the active probe used in this experiment is less than 1 mm in diameter, we can postulate that we would obtain a similar response if the probe was scanning directly over an equivalently tight crack having a length of 1 mm. From this we can conclude that the sensitivity of the FMR-MEC method is reduced as the flaw becomes tighter, since an open notch of 0.42 mm in length produces an equivalent response magnitude in the mixed data. However, it appears from these data that the FMR-MRC method has the sensitivity to detect tight cracks in the order of 0.5-1.0 mm in length and 1-3 microns in width in Ti 6-2-4-6 or IN-100 materials.

2.1.4   Development and Characterization of Active FMR Probes

2.1.4.1   Some Introductory Active FMR Probe Oscillator Theory

For the active FMR probe, conditions for strong oscillation can be expressed as

$K < 1$

$1/S_{11}' = \Gamma_R$

$1/S_{22}' = \Gamma_L$

16

The stability factor K for the oscillator circuit must be less than unity and in the case of the common-base oscillator configuration, its emitter must resonate with the FMR probe ($1/S_{11}' = \Gamma_R$) and it's collector must resonate with the load matching circuit ($1/S_{22}' = \Gamma_L$). The latter two equations can be combined into the form

$$\Gamma_R = \left[S_{11} + \frac{S_{21}S_{12}\Gamma_L}{1-S_{22}\Gamma_L} \right]^{-1}$$

where S_{11}, S_{21}, S_{12}, and S_{22} are the scattering parameters for the transistor, including any feedback circuitry, Γ_L is the load reflection coefficient, and Γ_R is the resonator (FMR probe) reflection coefficient. From this we can see that when the FMR probe reflection coefficient (Γ_R) changes as a result of a flaw and/or liftoff fluxuation, Γ_L must respond accordingly or a mismatch will exist at the transistor output and/or input, weakening the conditions for oscillation, and thus changing the output amplitude. Since the load matching circuit is made up of fixed components, it can only change, in terms of Γ_L, when the oscillator frequency changes. Therefore, it is evident that the frequency dependent characteristics of Γ_L strongly influence the active FMR probe amplitude and frequency responses to flaw and liftoff.

In order to investigate this complex relationship, Battelle purchased an electronic circuit computer-aided-design (CAD) program that will work in terms of scattering parameters, reflection coefficients, and strip lines. Utilizing this CAD program along with experimental data, we attempted to directly correlate the oscillator circuit design and the FMR probe equivalent circuit flaw and liftoff responses with the ultimate flaw sensitivity and flaw/liftoff phase separation of the active FMR probe. This relationship is the key to fabricating active FMR probes with widely different YIG sphere/permanent magnet configurations. However, we were not successful in the correlation effort, since the CAD program is for linear circuits and does not analyze oscillators well.

2.1.4.2 Active FMR Probe Oscillator/Buffer Design for Dual probe Configuration

A dual active FMR probe was fabricated using the circuit shown in Figure 14. The oscillator section of this circuit (to the left of R_1) is a design developed for wideband operation into a 50 ohm load. The buffer stage around the 2N6701 transistor was added to allow wideband operation into a double-balanced mixer having a frequency dependent VSWR of the order of two. Oscillator to mixer isolation was achieved and wideband operation

17
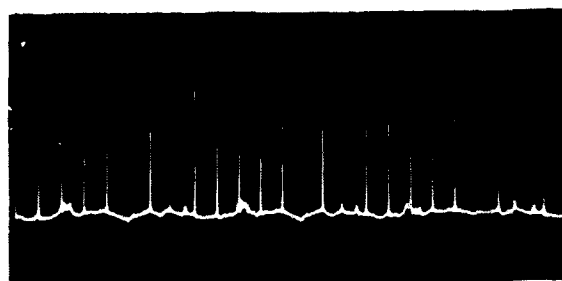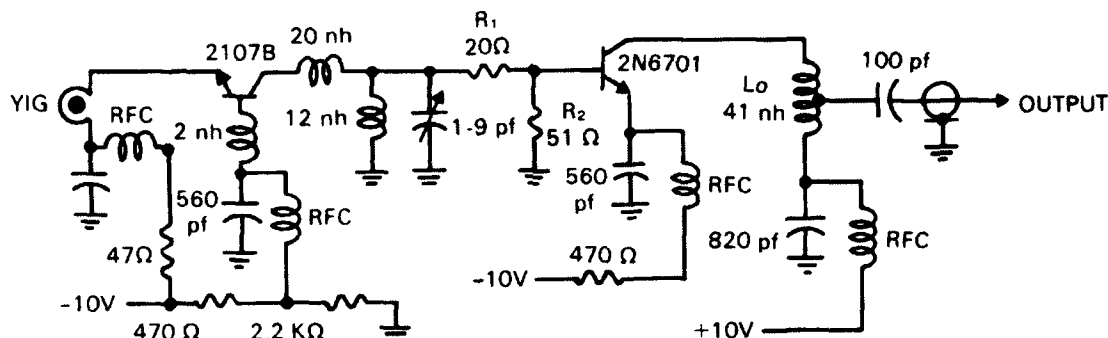
MIXED DATA ON THE
Ti 6-4 DISK

Figure 14. A Wideband Oscillator/Buffer Design.

maintained by adjusting R_1, R_2, and L_o. This buffer circuit was designed prior to our purchase of the CAD program. The dual probe was fabricated so that both FMR probes were in the same external dc magnetic field supplied through pole pieces from a permanent magnet.

We were unable to obtain both sides of the dual probe to operate simultaneously for differential evaluation. This was due both to mechanical and electronic deficiencies. Mechanically we were unable to adjust both YIG spheres for proper orientation in the external field without causing large liftoff discrepancies. This can be remedied with a more versatile YIG sphere adjustment mechanism. Electronically we were unable to get a desirable level of amplitude sensitivity from either probe. We suspect this to be caused by the gain characteristics of the buffer stage. This feeling was later substantiated by a gain analysis generated by the CAD program on the buffer circuit

18

revealing a highly frequency dependent gain function. This could easily affect amplitude information in a signal where frequency is fluxuating with amplitude.

The mixed data, shown at the bottom of Figure 14, was taken with one side of the dual probe scanning the Ti 6-2-4-6 disk. Even with weak amplitude information, it was possible to adjust the probe, signal processor, and mixer for an adequate flaw-signal to liftoff-noise ratio. However, the adjustments were much more critical because of the weaker data.

Based on the repeatability of the active FMR probe sensitivity demonstrated with five probes in our previous FMR-MEC project,[3] we feel that with some basic improvements in electronic and mechanical design, the dual-differential FMR probe configuration could be a practical way of achieving liftoff signal suppression. However, its size, which is approximately double that of a single probe, will prohibit its use in some tight turbine engine geometries.

2.1.4.3 Active FMR Probe Design with Fewer Electronic Components and Without Magnetic Pole Pieces

The active FMR probe, shown in Figure 15, was designed and fabricated to evaluate factors involved in probe miniaturization. Ideally we would like to operate a single active FMR probe constructed with electronic chip components and a DC magnetic field source consisting of a single miniature *samarium cobalt* permanent magnet without bulky pole pieces. A miniaturized configuration could solve flaw detection problems practically independent of geometrical restrictions. The probe in Figure 15 was fabricated with chip components, except for the inductor's and tuning capacitor, which would be replaced with a chip once an optimum value was determined. Space was provided for a single 6.25 mm permanent magnet with room to reposition it to produce various field directions and magnitudes.

The data, shown in Figure 15, illustrates the flaw responses at various liftoff settings with the liftoff response, shown below, plotted from 0.25 mm on the left to zero liftoff on the right. The flaw responses are from the Ti 6-4 disk shimmed for 0.025 mm liftoff fluxuation per revolution. We can see that even though the flaw responses are strong at the lower liftoff settings, the curvature of the liftoff locus will prohibit adequate liftoff suppression in the mixed data without the use of nonlinear mixing techniques. When we compare these data to those from a previous probe design with pole pieces (see Figure 8) and take into account the fact that both probes are electronically equivalent by design, it is evident that the difference in their liftoff responses is primarily a result of their

19

SINGLE
6.25 mm
PERMANENT
MAGNET

LEAVE
ROOM FOR NEW
BUFFER

470 pf   YIG   2107B   0.5-2.5 pf   50 Ω   TRL   OUTPUT

100 Ω   4 nh   8 nh
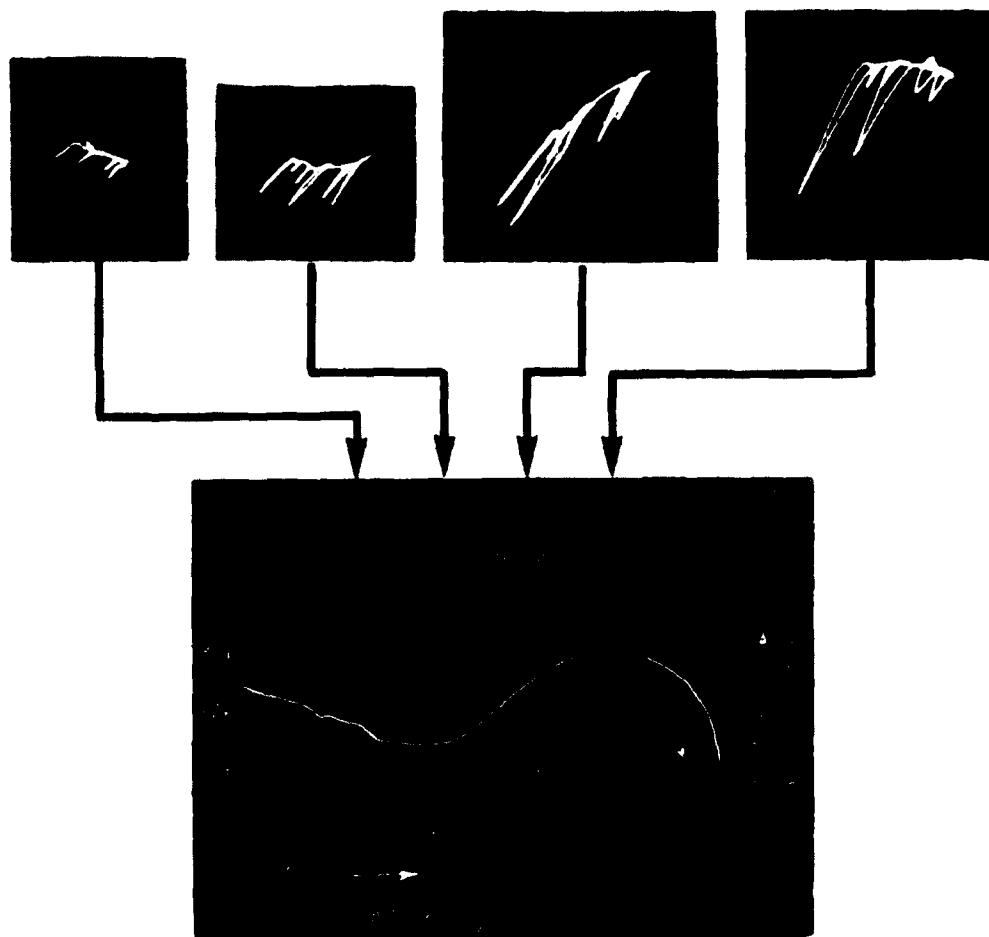
1.5 k

0.1μf   5.1 k   470 pf

-12 v
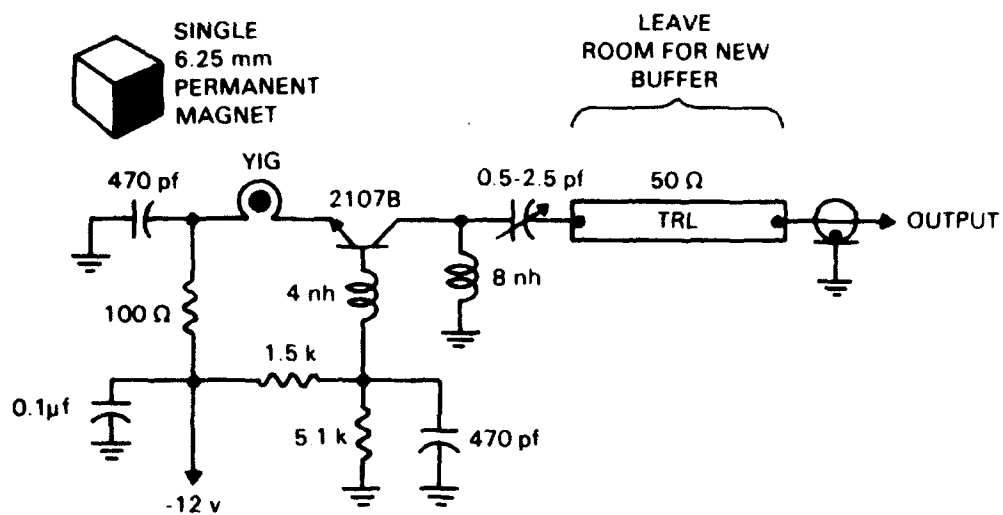
Figure 15.   Active FMR Probe Design Without Pole Pieces.

differing DC magnetic field configurations. As discussed earlier in this report, it is theoretically possible to modify the oscillator circuitry in such a way as to provide the desired flaw and liftoff responses for a wide range of DC magnetic field configurations. We feel that an analytical approach exists for determining the optimum circuit design for flaw/liftoff separation.

With liftoff suppression as a primary concern, it should be noted that for certain applications it may be possible to aero-mechanically stabilize liftoff with an air bearing like that currently being studied at Southwest Research Institute of San Antonio, Texas. This would allow the use of the FMR-MEC method in an extremely sensitive and mechanically simple configuration.

2.1.4.4 Improved Buffer Design from CAD Program

As it applies to the FMR-MEC method, a good buffer design provides isolation from the double-balanced mixer and does not distort the data. With these characteristics in mind, the buffer circuit shown in Figure 16 was designed, fabricated and evaluated. The circuit configuration with initial values was entered into the CAD program with the design goals of an input VSWR <1.05 and a gain of 0 dB from 600 to 1100 Mhz. The CAD program then adjusted the circuit values to obtain the design goals. We fabricated the circuit using realizable circuit values as close to the optimized values as possible. The circuit was then tested for input VSWR, which measured less than 1.06, and gain, which
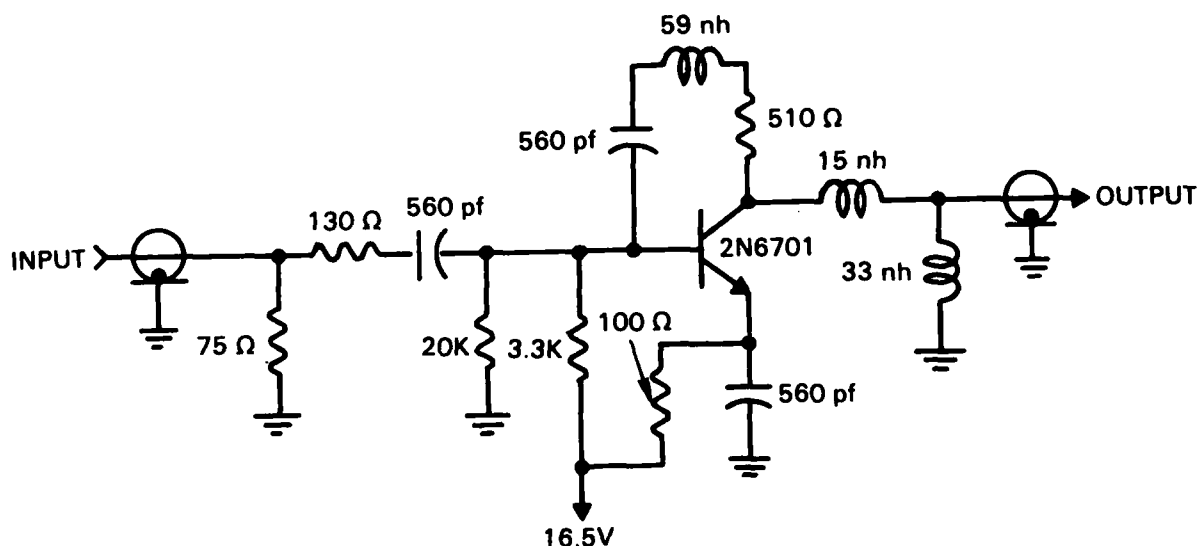
Figure 16.   Improved Buffer Design.

measured a constant -2 dB across the 600 to 1100 MHz band. Even though there is a discrepancy in the absolute gain of the buffer from the design goal of 0 dB, we feel that the design is a success for our application, since the gain is independent of frequency.

2.1.5 Constraint Analysis Related to Jet Engine Interstage Seal Key Slot Inspection

The jet engine interstage seal component, shown in Figure 17, was sent to Battelle by the Air Force Contract Monitor. The region of interest is the key slot which serves to transfer the rotational forces of the turbine to the component. We have chosen the inside radius corner of the key slot for inspection with our complex geometry probe. This geometry selection was based on the difficulty of getting a probe into the key slot and performing a scan of the total corner area. We also feel that development of such a probe will generate the technology necessary to fabricate probes for other geometries such as the 3 mm diameter cooling holes.

A detailed geometry of the key slot region is shown in Figure 18. As illustrated, the radius of the key slot corner is 1.8 mm. In order to scan this geometry, the probe must be less than 3 mm in diameter. The cross section view of the key slot region also illustrates the geometrical restrictions on the probe on either side of the key slot. We have selected the

Figure 17. Jet Engine Interstage Seal Component.

22
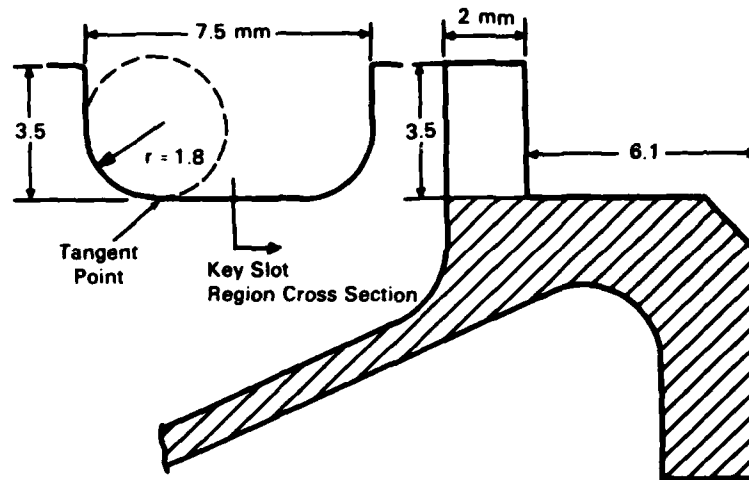
Figure 18. Key Slot Region Detailed Geometry.

approach of entering our probe from the right side of the cross
section view. This approach provides the least geometrical
restrictions on the size of the MEC signal processor, which
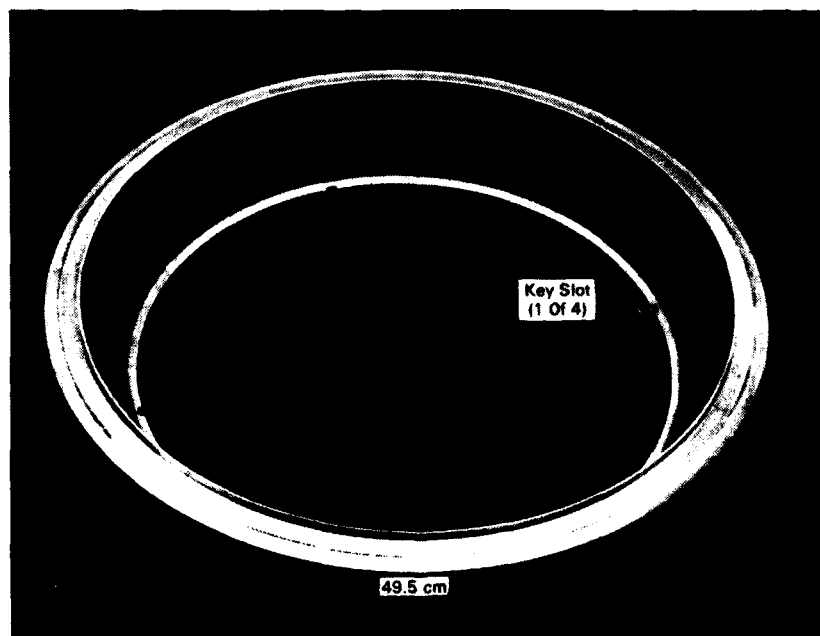connects directly to the inspection probe. In terms of active
FMR probe design, this geometrical restriction impacts two as-
pects of the design: 1) the probe oscillator circuit design and
fabrication, and 2) the DC magnetic field source, or permanent
magnet, design, and fabrication.

2.1.6 Analysis and Development of Methods to Geometrically Shape the Active FMR Probe

2.1.6.1 Operational Input Resonant Condition Analysis of Active FMR Probe

In order to relate the effects of reshaping the geometry of
the active FMR probe to its performance, we performed an in-depth
experimental analysis of its operational input resonating con-
ditions. To accomplish this, we utilized an oscillator circuit
with an AC model as shown in Figure 19. This model is typical
of our most sensitive probe oscillator designs. By connecting
various series RC or RL chip or wire component combinations
between the oscillator transistor emitter and ground and mea-
suring the resultant oscillator frequency, we were able to
generate a plot of the oscillator's operational frequency as a
function of its input circuit. As shown in Figure 20, the input
circuit is characterized in terms of its reflection coefficient
(Γ_R) on a 50 ohm Smith chart. Also plotted is a hypothetical FMR
probe reflection coefficient. All frequencies on these plots
are in megahertz. If an actual FMR probe having a Γ_R plot as shown
in the figure were connected to the emitter of the oscillator

23

Figure 19. AC Model of a Typical Active FMR Probe.

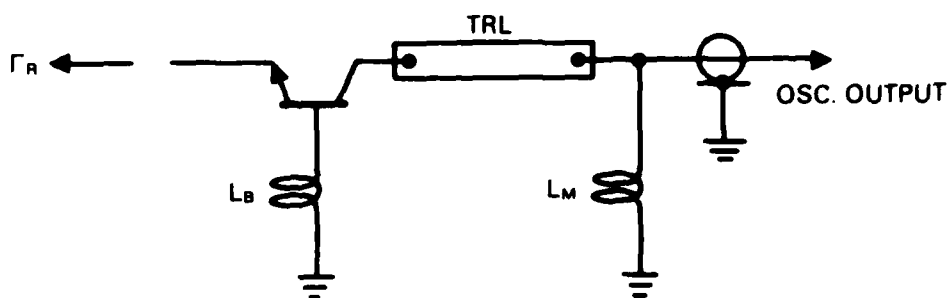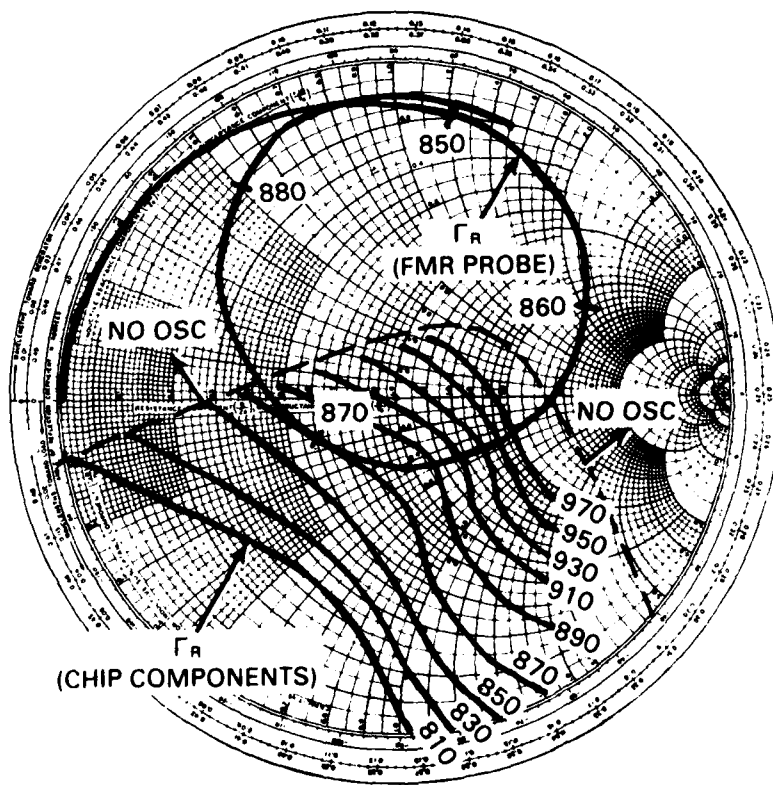Figure 20. Active Probe Oscillator Frequency Characteristics as a Function of the Emitter Circuit.

24

used in this analysis, the resultant active FMR probe would resonate at 870 MHz. As we can see in Figure 20, the FMR probe satisfies the operational input resonant condition of the oscillator at 870 MHz and nowhere else in this example. This is primarily due to the high Q of the FMR probe, which provides only about 10 MHz of Γ_R locus in the region on the chart where oscillator input resonance can occur. In this example of input resonance, the FMR probe locus is tangent to the constant frequency Γ_R locus for 870 MHz. Input resonance and thus oscillation would also occur if the magnetic flux density at the FMR probe were increased to cause the Γ_R locus of the probe to be located at 970 MHz where it crosses the 970 MHz constant frequency curve. We feel that the angle at which the FMR probe Γ_R locus intersects the constant frequency curve at the point of resonance primarily determines the active FMR probe's sensitivity. This concept is very difficult to evaluate experimentally at these frequencies, since it is impossible to analyze sections of an active probe, such as the FMR probe, without disturbing them electrically.

The active FMR probe's input resonant condition and thus sensitivity can be adjusted by either manipulating the FMR probe and its DC magnetic field or changing the input resonant conditions of the oscillator with its circuit components. By far the most sensitive adjustments occur in the YIG/dc magnetic field arrangement in terms of the field strength, direction, and uniformity. As geometrical restrictions are put on a probe *design*, these become the only practical adjustments available during probe fabrication. However, with these restrictions the field strength and uniformity become very critical due to the relatively high flux density gradients associated with small permanent magnets. Also of primary concern is the fact that high flux density gradients reduce the FMR probe Q. On the Smith chart this would be observed as a reduction in the size of the loop formed by the FMR probe $_R$ locus at ferromagnetic resonance. As the Q approaches zero, the resonance loop would approach a point near the perimeter of the chart and the Γ_R plot of the FMR probe would merely be that of its coupling loop inductance. Therefore, we can see that maintaining an adequate FMR probe Q is critical to active probe operation. We have investigated techniques which will effectively keep the FMR probe Γ_R locus in the operational input resonant Γ_R region for lower FMR probe Q conditions that are inherent to small diameter probe designs *such as the key slot corner inspection probe.*

2.1.6.2 Transmission Line Techniques Applied to Active FMR Probe Miniaturization

We have utilized a computer-aided-design (CAD) program along with the equivalent circuit model of the FMR probe to investigate techniques for achieving active FMR probe operation in geometrically restricted designs. The most detrimental effect of probe miniaturization on probe performance is the loss of FMR probe Q. This effect occurs when the probe's DC magnetic source, or permanent magnet, is also miniaturized. A reflection coefficient locus of an FMR probe is shown in Figure 21. This plot was CAD generated at frequencies from 300 to 1300 MHz. The FMR probe has a Q of approximately 155 and a coupling loop inductance of 7 nh, which includes 4 nh for leads. For this
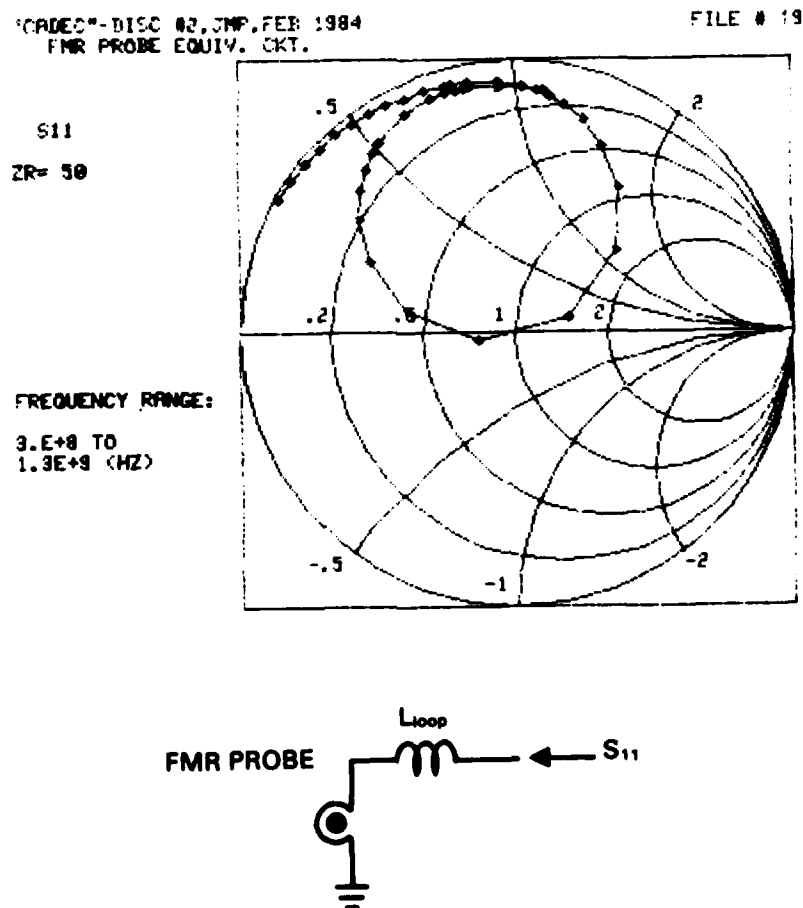
Figure 21. CAD Generated Reflection Coefficient Locus of an FMR Probe.

configuration, the probe's reflection coefficient locus scarcely moves into the lower half of the chart, where most of the desired input resonant conditions exist.

A technique designed to physically extend the FMR probe away from the oscillator circuitry while increasing its apparent Q is shown in Figure 22. In this configuration each transmission line (TRL) is 12.5 mm of 50 ohm stripline on 1.5 mm thick phenolic substrate and the capacitors are each 10 pf. For the FMR probe the Q is the same as in Figure 21 but the loop inductance was reduced to 3 nh, assuming that the loop would be connected directly to the stripline and ground plane, reducing the requirement for leads. As we can see, the Q has apparently increased and more of the FMR probe's reflection coefficient
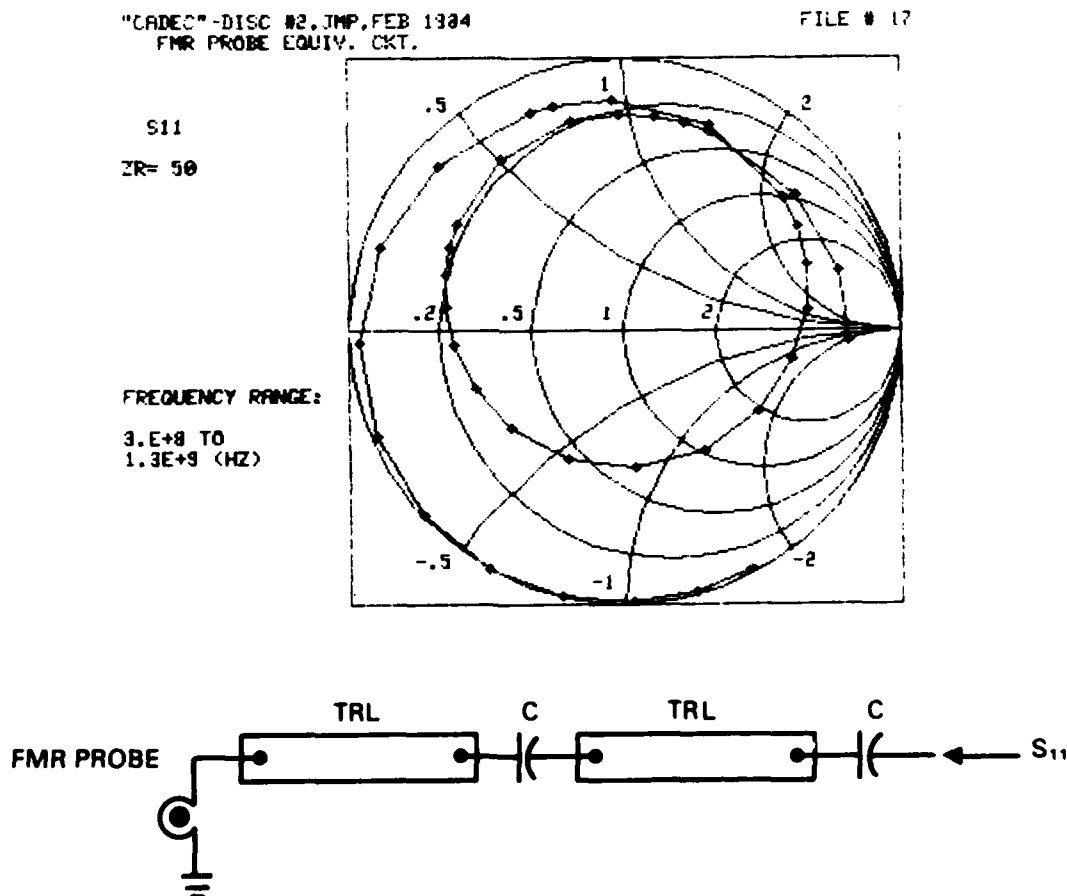
Figure 22. FMR Probe Extension Technique on Phenolic Substrate.

27

locus is located in the lower half of the chart. Note that the plot starts at 300 MHz along the bottom perimeter of the chart and ends at 1300 MHz just into the bottom right section of the chart. Conceivably, there are three regions in the reflection coefficient locus that could satisfy the input resonant condition of the oscillator. The effect of this occurring is a highly distorted oscillator output. To insure that it does not happen, care must be taken in the design to make sure that only the loop-shaped locus of the FMR probe's reflection coefficient at ferromagnetic resonance is at frequencies coinciding with the operational frequency range of the oscillator circuit. This extension technique has been successfully implemented on one of our latest oscillator circuits. However, we did experience difficulties in eliminating secondary oscillations at approximately 1300 MHz.

Another transmission line extension configuration is shown in Figure 23. It consists of TRL1, which is 2.5 mm of 50 ohm stripline, and TRL2, which is 2.5 mm of 20 ohm stripline. The substrate is 0.63 mm alumina. Note that this arrangement does not have unwanted sections of its reflection coefficient in the lower half of the chart. The thin alumina substrate is well suited for miniaturization of stripline circuitry. For example, in most of our experimental work we use 1.5 mm thick phenolic board, which requires a 3 mm wide stripline for a 50 ohm characteristic impedance. A stripline width of only 0.5 mm is required on 0.63 mm alumina for a characteristic impedance of 50 ohm. We implemented this technique with particular success in a low Q small permanent magnet design that will be discussed later in this report.

2.2   DEVELOPMENT OF A BREADBOARD FLAW DETECTION SYSTEM (TASK II)

2.2.1   Development of Small Radius Active FMR Probes

2.2.1.1   Coax Type Probe Design

Since our active probe designs utilize transmission line impedance matching in their oscillator output circuits, we investigated the use of coax sections in the probe fabrication. Our approach consisted of replacing the 50 ohm stripline matching section seen in previous probe designs with an electrically equivalent section of 2.13 mm diameter 50 ohm rigid coax. Utilizing the network analyzer, we found that a length of 21.3 mm of the rigid coax was equivalent to the 18.8 mm of stripline that was in our existing probes. With this information, we fabricated and tested our first coax type probe shown in Figure 24. Also shown are data taken with the probe on our Ti 6-4 disk specimen. For this test, a 6.25 mm cube SmCo magnet (not shown) was used for the DC magnetic source. The data were taken with

28

S11

ZR= 50

FREQUENCY RANGE:

3.E+8 TO
1.3E+9 (HZ)
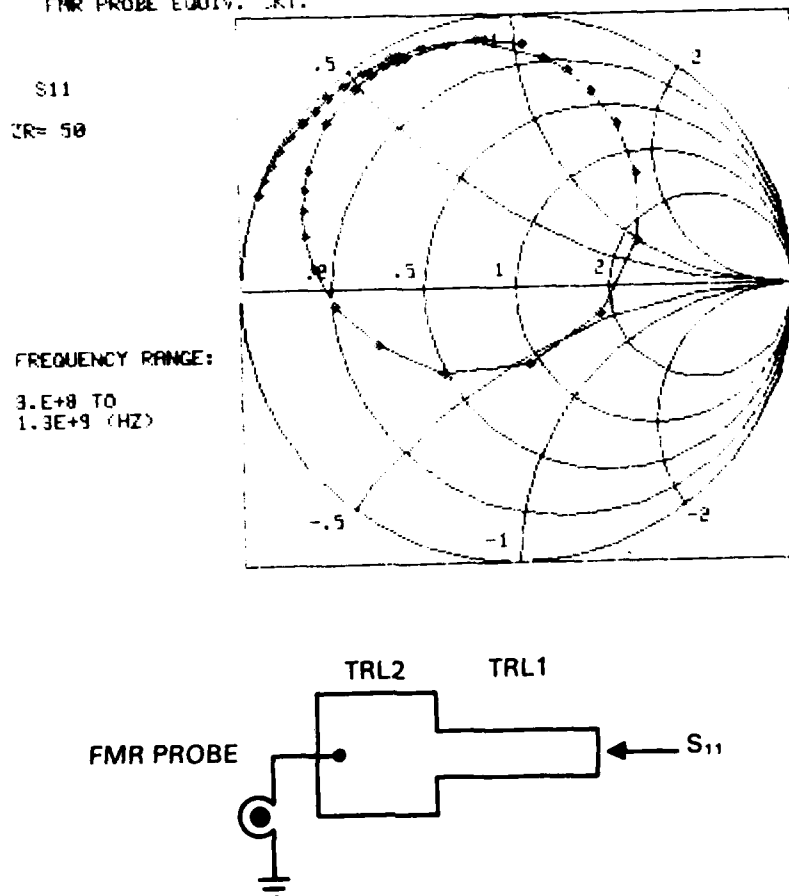
Figure 23. FMR Probe Extension Technique on Alumina Substrate.

the FMR probe potted to a 4 mm length of rigid coax, which was
the electrical connection between the FMR probe and oscillator
transistor. This probe performed well, considering that the YIG
was potted into the coupling loop prior to taking data, which did
not allow for any adjustments to enhance sensitivity.

    In the process of further miniaturizing the coax type probe
design, we modified its design, including changing to a smaller
oscillator transistor. As shown in Figure 25, we also cleaned
up its profile by putting the DC power for the oscillator on the
coax center conductor, which also carries the RF power out of the
probe.
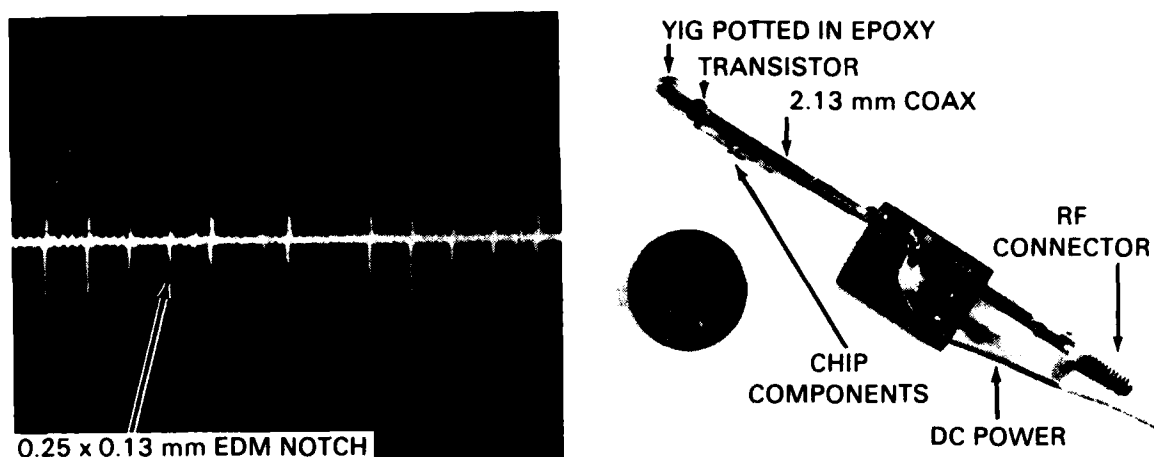
Figure 24. First Coax Type Probe.
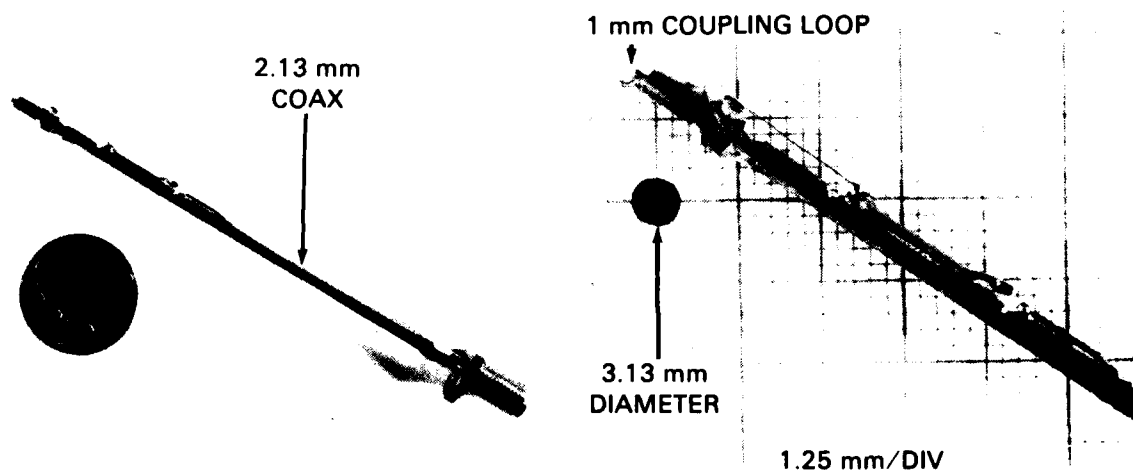
Figure 25. Second Coax Type Probe.

The schematic for this probe, shown in Figure 26, illustrates how the oscillator circuit was biased and decoupled using chip resistors and capacitors. This probe design demonstrated good oscillation characteristics but required further miniaturization, which we decided not to pursue, to be usable as a key slot probe.

2.2.1.2 Alumina Substrate Probe Design

Alumina substrate is frequently used in the fabrication of hybrid microwave circuit boards. This is primarily due to the alumina material's high dielectric constant which is in the order of ten. This relatively high dielectric constant helps reduce the dimensions of the circuit boards since the wavelength

30
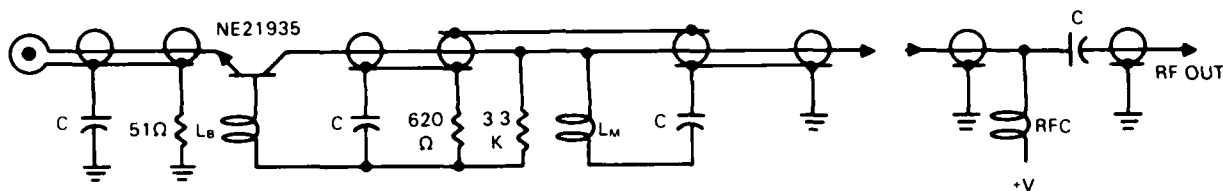
Figure 26. Schematic of Second Coax Type Probe.

on the board is inversely proportional to the square root of the dielectric constant. Stripline widths are further reduced by reducing the thickness of the substrate.

We utilized 0.63 mm thick alumina sheets which we had copper coated. A 50 ohm stripline on this arrangement is 0.5 mmm wide. The conceptual design of a probe for inspecting in a 3.5 mm diameter goemetry is shown in Figure 27. This arrangement, which we utilized for the key slot inspection, is based on a cylindrical SmCo permanent magnet, a 1.8 mm diameter miniature transistor package, and the 0.63 mm thick alumina substrate circuit board with chip resistor and capacitor components. As illustrated, this hybrid circuit fits into a 3 mm cylindrical volume, which makes this key slot inspection probe design a possible solution for inspection of 3 mm cooling holes as well.
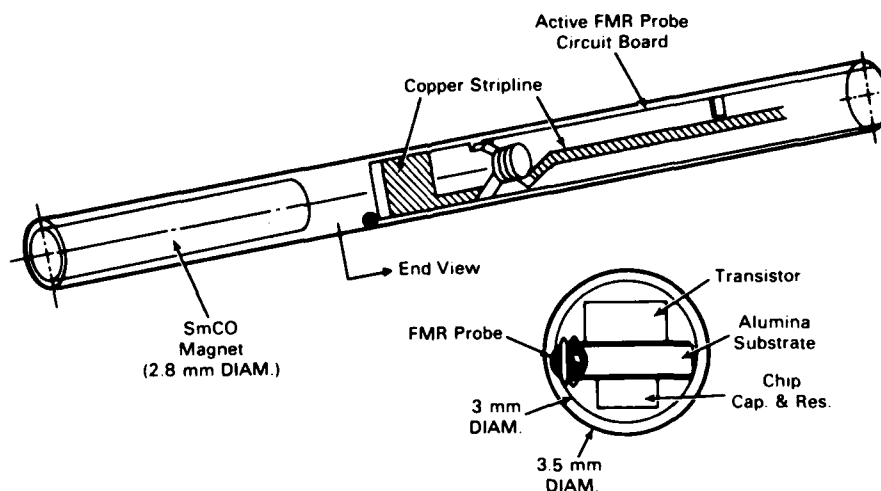
Figure 27. Conceptual Design of Key Slot Probe Based on Alumina Substrate Circuit Board.

31
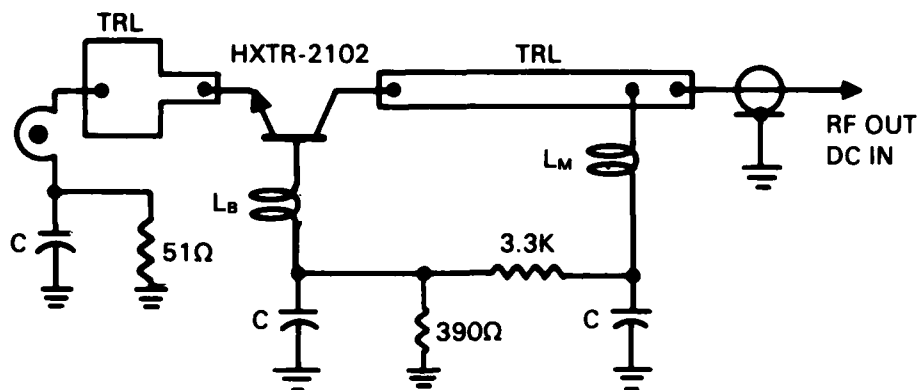
Figure 28.   Schematic of Alumina Substrate Probe.

Before fabricating a probe on alumina substrate, we fabri-
cated and tested on phenolic board the new oscillator design,
shown in Figure 28.   This design is based on the smallest
stripline package transistor we could find. We have found that
each transistor type used in the probe oscillator requires its
own unique DC biasing and RF matching circuit values.   For
example, the base inductor (L_B) from transistor to transistor
ranges from 2 nh to as high as 16 nh.   In terms of physical
dimensions, these values of inductance correspond to wire
lengths of 2.5 to 15 mm, respectively, which must be considered
during probe layout.   Note that the transmission line which
connects the transistor emitter to the FMR probe is similar to
a design discussed in Section 2.1.6.2 of this report under
transmission line techniques.   As previously discussed, its
purpose is to increase the apparent Q of the FMR probe in
applications where small permanent magnet geometries are re-
quired.

With the circuit elements established for good oscillation
characteristics on the phenolic board with a 7.8 mm diameter
cylindrical SmCo magnet as the DC magnetic source, we fabricated
the alumina substrate active FMR probe shown in Figure 29. Also
shown in this figure is a 2.8 mm diameter cylindrical SmCo
magnet. A detailed component layout of this probe is shown in
Figure 30. We positioned a YIG sphere in the FMR probe loop and
achieved good oscillation characteristics in the 700 to 900 MHz
frequency range.   We have found that once good oscillation
characteristics have been obtained that achieving the desired
flaw sensitivity becomes a function of the FMR probe/DC magnetic
field orientation.   Further evaluation of this design is dis-
cussed later in this report in the rotary probe section.

32
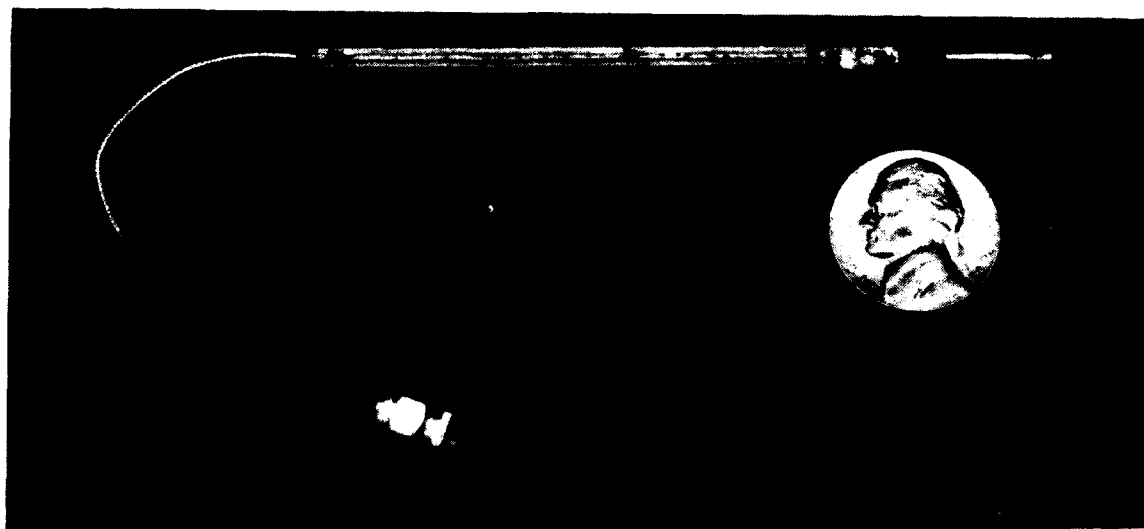
Figure 29. Alumina Substrate Active FMR Probe.

2.2.2 Development of Techniques to Simplify the Fabrication
       Process of the Active FMR Probe

   2.2.2.1 Enhanced FMR Probe Optimization Technique

   The most critical and most time consuming effort in the
fabrication of an active FMR probe is the orientation process of
the YIG sphere in the DC magnetic field during optimization of
probe performance. This is due to the complexity of the YIG
material magneto-crystalline anisotropy. In order to provide a
highly flexible, as well as controllable, method of optimizing
probe performance during fabrication, we developed the FMR probe
optimization technique shown in Figure 31. In this arrangement,
the FMR probe coupling loop and oscillator circuit are held in
a fixed position while the YIG sphere can be rotated and tilted
to obtain maximum sensitivity. The DC magnetic field can also
be adjusted in terms of its strength by adjusting the distance
between the permanent magnet and the FMR probe. While the
adjustments are being made, we can observe their effects on the
active probe's performance as an EDM notch is being scanned back
and forth under the FMR probe. The mechanical YIG and magnetic
field manipulator designed and fabricated for this technique are
shown in Figure 32. The YIG sphere is mounted on an alumina rod
and located in the position shown in the figure. The cylindrical
SmCo magnets fit into the magnet adjustment tube at the point
indicated. This device provides the necessary adjustment ranges
to locate the optimum FMR probe/DC magnetic field orientation.

33
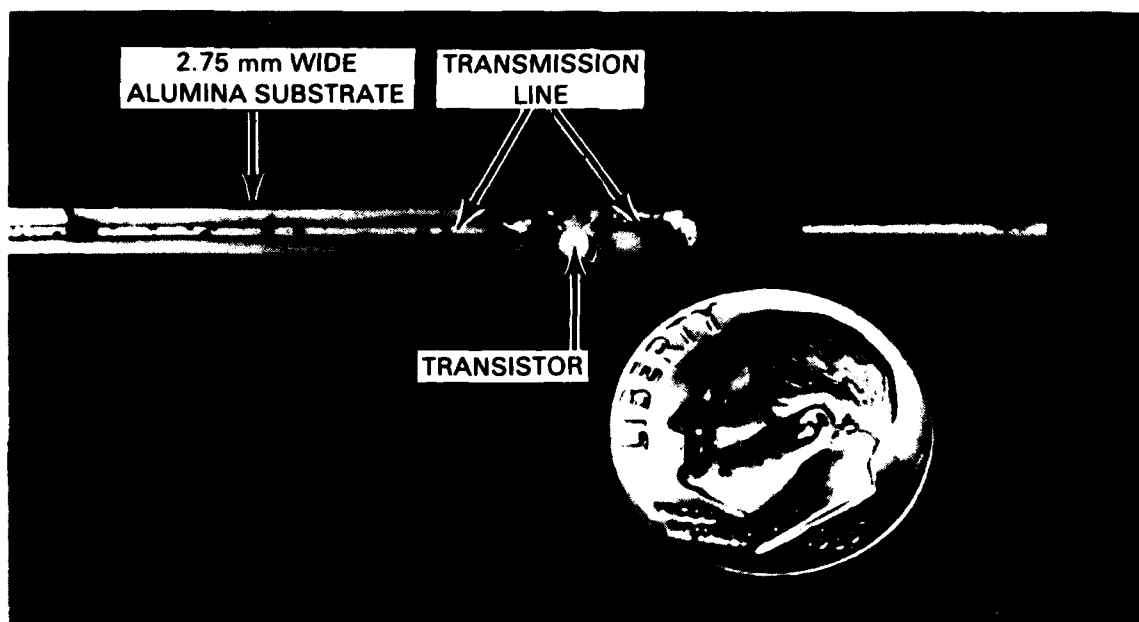
Transistor/Stripline Side

Chip Component/Inductor Side

Figure 30. Component Layout of Alumina Substrate Probe.

34
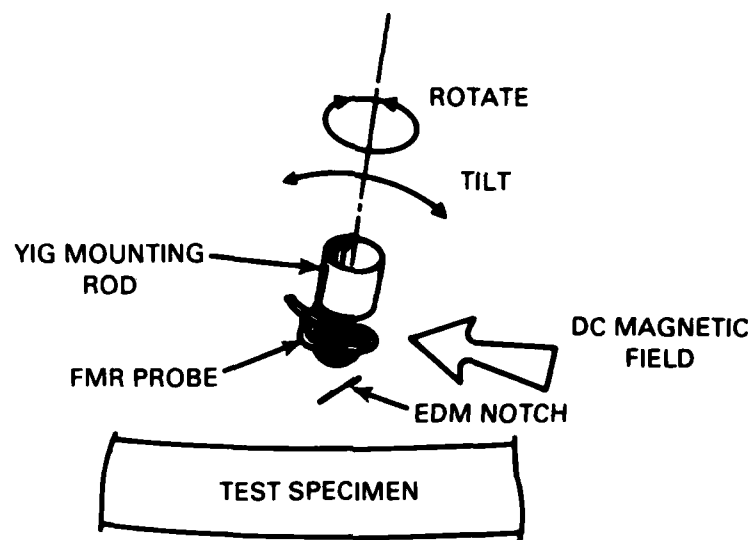
Figure 31.   FMR Probe Optimization Technique.
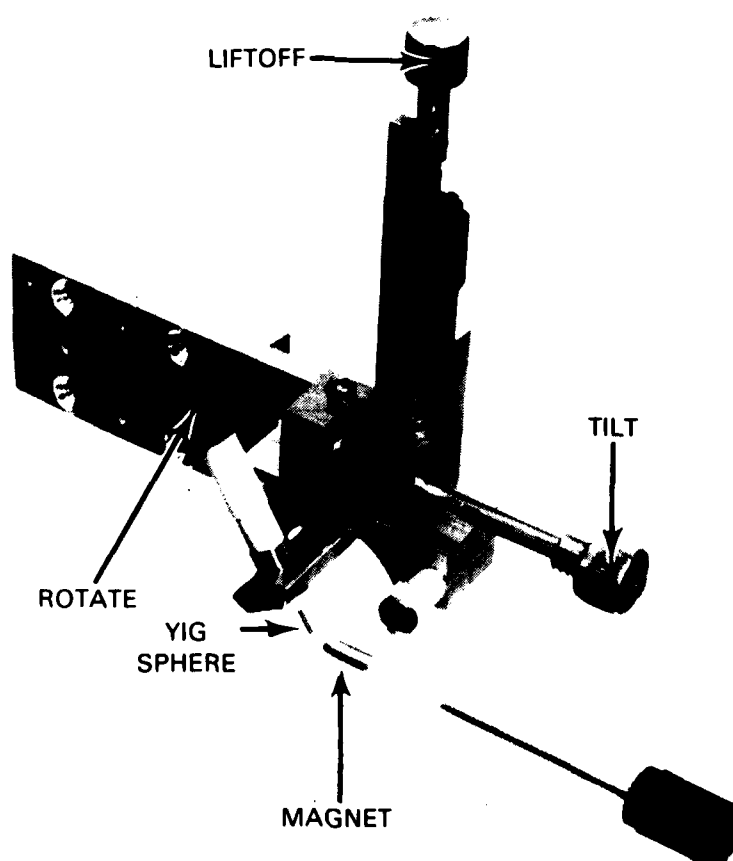
Figure 32.   FMR Probe YIG and Magnetic Field Manipulator.

2.2.2.2 Active FMR Probe with Ferromagnetic Resonator in the Base Circuit

We evaluated the possibility of significantly changing the active FMR probe's oscillator design so that it would operate with a wider range of resonator reflection coefficient conditions. We initially evaluated the approach on our microwave circuits CAD program. The approach puts the FMR probe in the base of the oscillator transistor and resonates the emitter with a series RC network. Our normal design has an inductor in the base and resonates the emitter with the FMR probe. The CAD analysis we performed indicated that the oscillator should respond strongly to changes in FMR probe resonant frequency and Q. Also, it appeared that it would be fairly easy to set the RC network in the emitter to resonate the circuit over a wide range of FMR probe reflection coefficients. This technique would electronically tune the oscillator circuit to fit the FMR probe characteristics rather than mechanically adjust the FMR probe to fit the oscillator input resonant characteristics. We performed an experimental evaluation on the active FMR probe design shown in Figure 33. The circuit proved to be very difficult to tune up for FMR operation. Our CAD program had predicted that the RC network in the emitter would resonate the circuit; however, it did not indicate that the circuit will oscillate at much less than ideal conditions, due to the nonlinear large signal characteristics of the transistor. Thus the difficulty with this circuit is tuning it so that it oscillates only when the FMR probe is resonating. This was accomplished with R_E = 10 ohms and C_E = 10 pf. As predicted by the CAD program, this circuit will
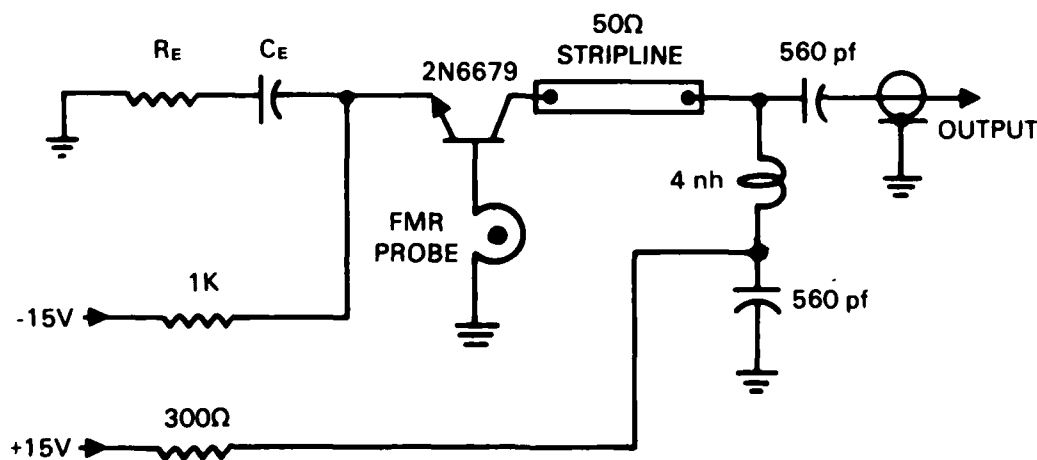
Figure 33.   Schematic of Active Probe with FMR Probe in the Base Circuit.

operate with a longer FMR probe loop lead and with less resonator Q, which are desirable characteristics for a physically small probe configuration. However, the probe's flaw sensitivity was significantly less than that of our previous probe designs. We believe this is primarily due to this circuit's high instability, which tends to constantly pull the oscillator frequency and reduce the effects of the FMR probe.

2.2.3 Development of Rotary Probe Inspection System

2.2.3.1 Rotary Probe Concept

The conceptual design of the rotary probe is shown in Figure 34. This concept is designed to permit active FMR probe rotation for scanning the key slot corner geometry. It can also be applied to bolt hole geometries as well as flat surface geometries. We included the design of an interchangeable flat surface scanning probe. We feel that demonstrating the concept of interchangeable active FMR probes is very important in establishing this test method's practical application in NDT. For either the small radius or the flat surface configurations, the active FMR probe is located entirely in the interchangeable probe attachments. When attached, the active probe RF output is transferred through an RF connector to the signal processor located in the rotating section of the rotary probe assembly.
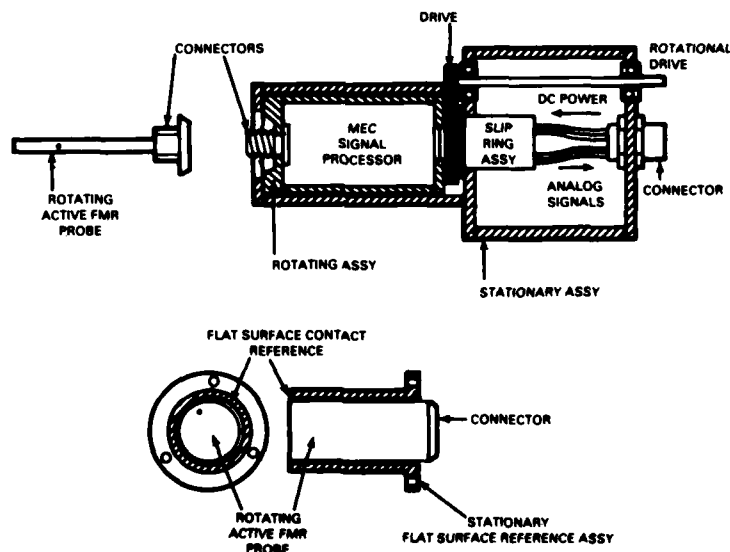
Figure 34. Rotary Probe Conceptual Design.

The small radius probe is designed for non-contact scanning of the key slot corner. The flat surface probe is designed for contact on the test material surface with the nonrotating reference surface of the probe attachment while the rotating active FMR probe is recessed for a noncontact circular scan.

2.2.3.2 Rotary Probe Signal Processor Concept

As shown in Figure 35, the signal processor converts the 800 MHz RF output of the active FMR probe to voltage levels corresponding to the amplitude and frequency of the probe output. These signals are transferred through a slip ring assembly to the stationary section of the signal processor assembly. For an industrial application, we would recommend the slip rings be replaced with a rotary transformer for increased reliability.
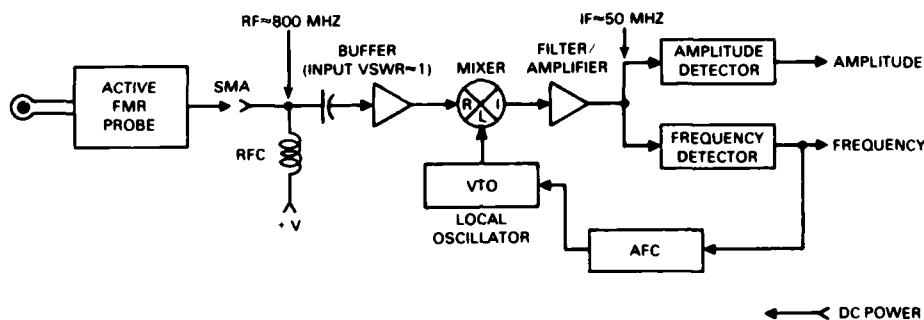
Figure 35. Rotary Probe Signal Processor Block Diagram.

The signal processor first converts the probe output signal frequency from 800 MHz to approximately 50 MHz while maintaining the relative amplitude and frequency information in the probe output. The amplitude and frequency detection circuitry is much simpler at the lower frequency. The frequency conversion is accomplished by mixing the probe output RF with a local oscillator RF signal set so that its frequency is approximately 50 MHz different than that of the probe. This produces a signal out of the mixer containing the sum and difference frequencies, 1650 MHz and 50 MHz, respectively. The sum frequency is rejected and the 50 MHz signal is passed onto the amplitude and frequency detectors for conversion to DC voltage levels corresponding to the relative amplitude and frequency of the probe output signal. The detectors are specifically designed to operate in a frequency range about the difference frequency. Automatic frequency control (AFC) is utilized in the signal processor to hold the difference frequency at approximately 50 MHz. However, the

AFC circuit time constant is sufficiently long to allow frequency changes to be observed on the frequency detector output. This feature is required in the rotary probe signal processor since we intend it to interface with differenct styles of active probes which are likely to have significantly different output frequencies, possibly exceeding 100 MHz.

2.2.3.3 Description of Finished Rotary Probe

The rotary probe which we used in the project final demonstration (Task III) is shown in Figure 36 with the interchangeable flat surface and small radius attachments. This design is based on the concept described earlier in this section. All machined components, except the ball bearings, are either aluminum or brass to minimize effects on the FMR probe DC magnetic field. Figure 37 shows the rotary probe disassembled to illustrate the major components. Not identified in this figure are the ball bearings of which there are two each located inside the small radius active probe assembly and two each located on either end of the signal processor boards.

The major components that go into the small radius probe attachment are shown in Figure 38. The active FMR probe consists of the alumina circuit board with the FMR probe wire loop, the YIG sphere, the permanent magnet and the RF connector. We used a 0.3 mm diameter YIG sphere in this probe. The outside diameter of the stainless steel tube is 3.3 mm.
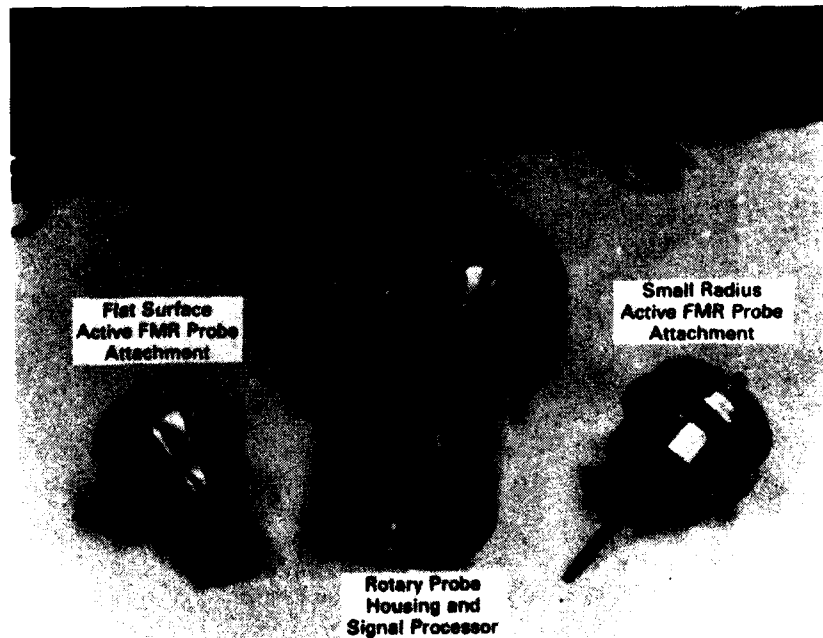
Figure 36. Rotary Probe with Interchangeable Attachments.

39
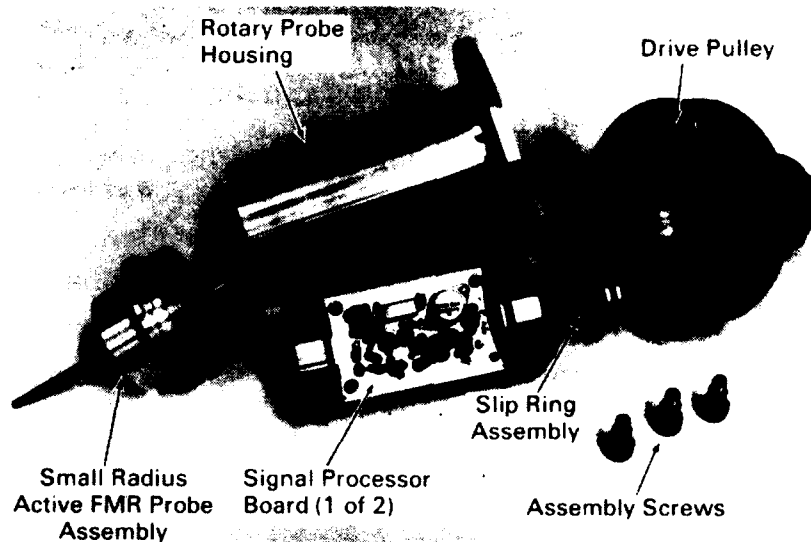
Figure 37. Disassembled Rotary Probe.
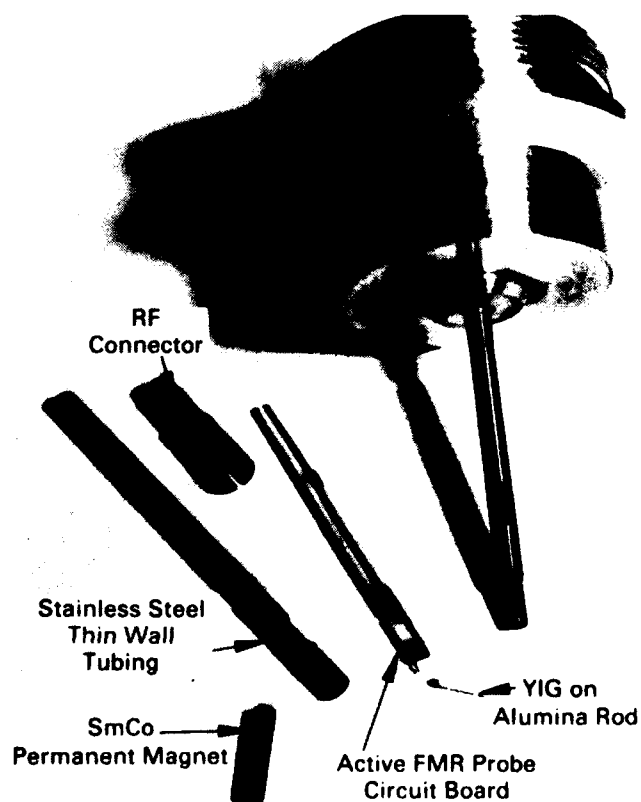
Figure 38. Small Radius Probe Components.

The flat surface attachment active FMR probe components are shown in Figure 39. In this configuration, we used a glass epoxy circuit board, a 6.25 cm cube magnet and a 0.75 mm diameter YIG sphere. The FMR probe location on the flat surface attachment provides for a 8 mm diameter circular scan.
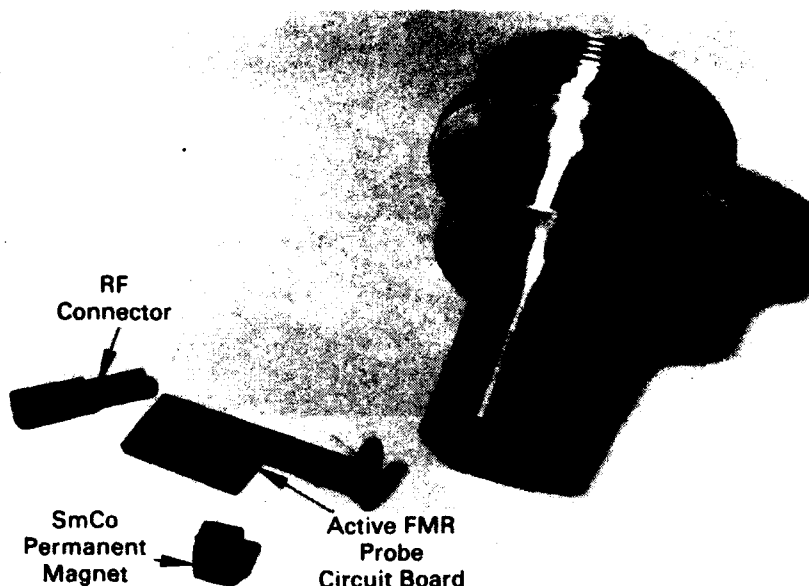
Figure 39. Flat Surface Probe Components.

2.2.4 Rotary Probe Laboratory Evaluation

2.2.4.1 Key Slot Inspection

The rotary probe is shown in the key slot inspection fixture in Figure 40. The small radius active FMR probe is positioned into the key slot corner with precision slides. Rotational drive is provided by a stepper motor driven flexible cable. The rotational speed of the probe is approximately 1.5 revolutions per second. Data taken with this arrangement are shown in Figure 41. The top trace in each of these data examples is the demodulated amplitude signal out of the rotary probe and the bottom trace is the amplitude signal bandpass filtered at 12-20 Hz. The data in the upper example are simply the liftoff response of the probe to an unflawed key slot corner. The lower-left example data are the probe response to a 0.25 mm x 0.13 mm EDM notch (RFC target flaw size), which was fabricated in the middle of the key slot corner. The flaw responses shown in the lower-right example are a result of a 0.75 mm x 0.13 mm EDM notch fabricated at the tangent point of key slot corner. We attempted

41
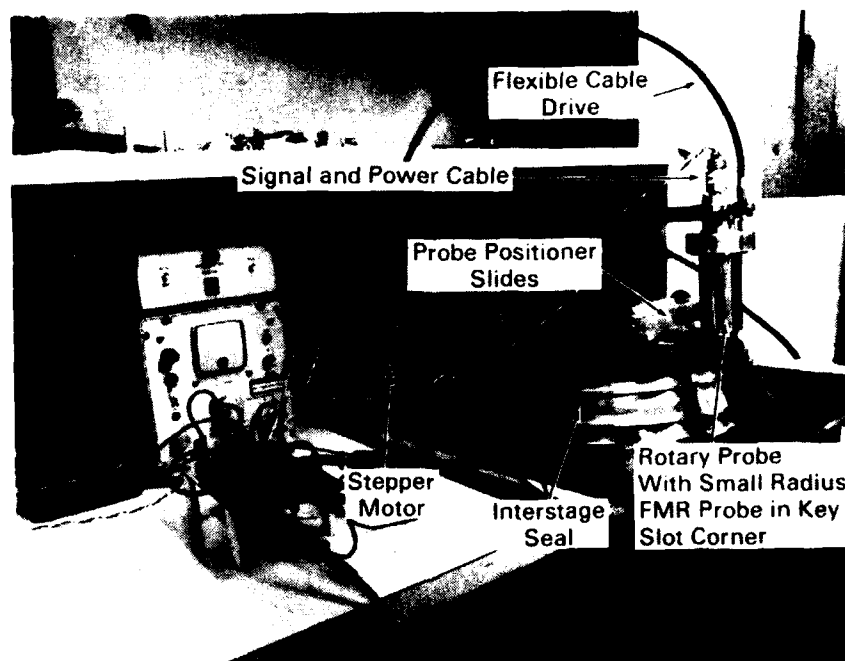
Figure 40.   Key Slot Inspection Arrangement.
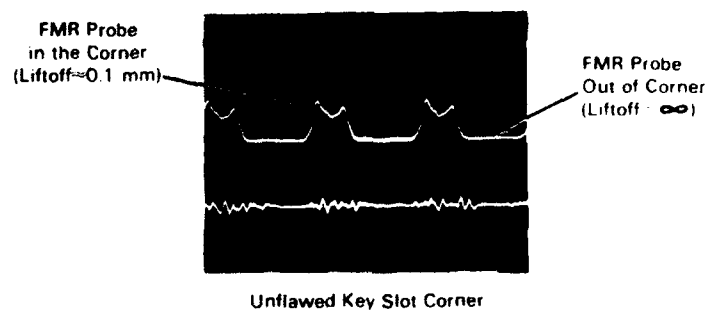
Figure 41.   Rotary FMR Probe Data from Key Slot Corner.

to detect a 0.25 mm x 0.13 mm notch fabricated near a target point with success. The notch was fabricated slightly out of the key slot corner and away from the tangent, which apparently resulted in excessive liftoff at that point in the rotational scan. Note that the flaw response in these examples is of equivalent magnitude to the liftoff response of the probe going from air, or infinite liftoff, to inspection liftoff, which is in the order of 0.1 mm. It is evident from these data that the extremely high operating frequency of the FMR probe (800 MHz) does not result in unacceptable liftoff responses even to worst case liftoff variations. We feel this is in part due to the extremely small effective eddy current field diameter (approximately 0.38 mm) of this probe.

2.2.4.2 Flat Surface Inspection

The rotary probe configured with the flat surface active FMR probe is shown in use in Figure 42. This figure illustrates the manual examination of a flat surface flaw specimen with the stationary probe housing in contact with the specimen surface. The rotating active FMR probe (refer to Figure 34 for flat surface probe concept) is recessed for a liftoff of approximately 0.1 mm.

Figure 42. Flat Surface Rotary Probe Operation.

Data taken with the flaw surface probe are shown in Figure 43. These data were developed by bandpass filtering the flaw response in the amplitude signal out of the rotary probe. The resultant flaw data illustrate excellent signal-to-noise responses to both the RFC target flaw size and a tight fatigue crack in Ti 6-2-4-6 material.

0.25 mm x 0.13 mm
EDM Notch
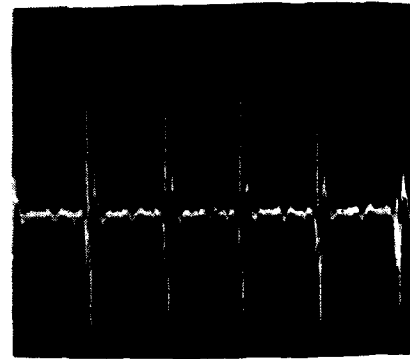
Tight Fatigue Crack

Figure 43. Flat Surface Probe Data.

44

3.0 THEORETICAL ANALYSIS AND MODELLING

(Stanford University)

3.1 BACKGROUND

In a previous contract for research in ferromagnetic probes (September 1980 to September 1982)[3] an investigation was carried out on basic design principles for the realization of a practical, properly engineered device. This work included a study of both single- and double-resonator probes, i.e., probes containing either one or two ferromagnetic resonance spheres. It was found that use of a double-resonator probe did provide some apparent improvement in the phase separation between the flaw and liftoff signals, and in an explicit and controlled manner. However, it was judged during the initial period of the present contract (September 1982 to September 1984) that the improvement was not sufficient to warrant going to the very significant increase in size and complexity of the double-resonator probe.

Earlier work at Stanford demonstrated the realizability of good phase separation in a single-resonator probe operating in the passive mode, i.e., an externally driven probe with input impedance readout. During the first year of development under the present contract, a corresponding degree of phase separation was achieved with an active probe, i.e., a self-excited oscillator probe with frequency and amplitude readout. In this case phase separation between the flaw and liftoff singls is observed in a frequency-amplitude plane display. The main thrust of the theoretical analysis and modeling activity under the present contract has been to provide scientific and technological information and guidance relating to the physical phenomena important in ferromagnetic probe design. This involved consideration of the following factors and a balancing of their effects to achieve optimum detection sensitivity:

- Amplitude-frequency liftoff discrimination.

- Dependence of the flaw signal trajectory in the impedance (or amplitude-frequency) plane upon magnetic bias field configuration and on YIG sphere crystal orientation.

- Influence of spurious magnetostatic modes.

- Physics and technology of magnetic crystal anisotropy.

- Limitations imposed by spin wave instabilities.

45

- Differences in the response of fatigue cracks and EDM notches.

- Optimum choice of probe design parameters.

In the present contract these topics were approached not for the purpose of increasing physical understanding, which is already rather complete, but rather for the purpose of incorporating this knowledge into the design of practical probes.

3.2   PRACTICAL DESIGN CONSIDERATIONS

3.2.1   Flaw-Liftoff Separation in the Frequency-Amplitude Plane

At the beginning of development under the present contract, the failure to observe flaw-liftoff separation in active probes under the previous contract was not understood, since the theory clearly predicted such a result. The difficulty could reside in the probe itself, in the transistor itself, or in a combination of both. An important task for the current contract's effort was therefore to identify the probe-related and transistor-related factors contributing to poor liftoff discrimination. For this reason, it was planned that Battelle test their probes in a passive mode with their new instrumentation before assembling in an oscillator. This would involve, say, measuring the liftoff ΔZ and the flaw ΔZ for some easy-to-detect flaws like sawcuts in aluminum. If liftoff discrimination is not observed in the passive probe, it cannot occur in the active probe, so that a properly operating probe must be constructed before insertion in the oscillator. Probe experiments were concurrently begun at Stanford to provide guidance on probe adjustment and, if necessary, to transfer a passive probe with good liftoff discrimination to Battelle for testing in an oscillator circuit. This part of the Stanford activities was terminated when active probe liftoff discrimination was achieved at Battelle during the first year of the contract.

3.2.2   Shape of the Flaw Signal Trajectory

In earlier research performed at Stanford on passive probes, it was observed that the flaw signal trajectory in the impedance plane could be changed from a line to a tear-shaped loop depending on the orientation of the DC magnetic field and the orientation of the YIG sphere. Since impedance plane trajectories for a passive probe translate into corresponding frequency-amplitude plane trajectories for an active probe, engineering design of the active probe requires understanding of this effect.

46

Experiments have been performed at Stanford for this purpose. Clear evidence was found showing that the differences are caused by probe asymmetry due to the DC magnetic field orientation and the crystal sample orientation with respect to the plane of the flaw, as first postulated. Consider a sample with the Z axis normal to the surface and a machined slot in the XZ plane. The probe used in the experiment had a DC field at an oblique angle to the surface of the sample and was scanned along the Y direction. Repeated scans were made with the oblique DC field rotated by various angles with respect to the plane of the flaw (i.e., the XZ plane). In general, tear-drop signal trajectories were observed, but the width of the tear-drop loop varied with the angular orientation of the probe relative to the plane of the flaw and the loop closed completely for one particular angular orientation. It is interesting to note that this did <u>not</u> occur when the tilted DC magnetic field of the probe lay parallel to the plane of the flaw, demonstrating that the magneto-crystalline anisotropy of the <u>unoriented</u> YIG sphere was also contributing to the probe asymmetry. This is a subject requiring further investigation, as it is not yet clear whether an open (i.e., tear-drop) or a closed flaw signal trajectory is more desirable in practice. The open trajectory is more like the signal obtained from a standard differential probe and may have similar advantages. In any case, this phenomenon provides a reason for carefully orienting the YIG spheres used in probe fabrication.

3.2.3 Influence of Spurious Magnetostatic Modes

In previous research at Stanford,[4,5] evidence was found that excitation of the ferromagnetic resonator in a combination of the uniform precession resonance and a secondary magnetostatic mode resonance appeared to enhance phase separation between the flaw and liftoff signals. This evidence concerning the significance of operating the probe simultaneously in two resonant modes was supported by experiments performed at Stanford under a previous contract (September 1980 to September 1982), and described in the Final Report.[3] Experiments performed at Battelle on the active probe confirmed, during the first year of the current contract, that careful orientation of the DC magnetic field and the YIG resonator does produce good flaw-liftoff separation in the active probe. Although the experimental evidence is very clear, quantitative characterization of the adjustment procedure (identification of the secondary magnetostatic modes involved, and establishment of the scientific principles governing the adjustments) remains elusive. To resolve this question, an intensive program of correlated theory and experiment would be required. Since the goal of this contract is to fabricate and demonstrate engineered ferromagnetic resonance probes, it was judged that the resources

47

of the contract would be better dedicated to these practical
goals than to generating this basic scientific understanding.
Adjustment of a probe for flaw-liftoff separation can be
achieved empirically and this is sufficient at the present stage
for the fabrication of probes.   In the future, more efficiency
in the fabrication process may require a deeper understanding of
the underlying physics.

3.2.4 Magnetic Crystal Anisotropy

Orientation of the YIG crystal sphere in the probe struc-
ture is of engineering importance for the reason noted under
3.2.2 above, as well as to provide: 1) probes with reproducible
characteristics from unit to unit, 2) compensation of probe
characteristics against variations in ambient temperature, and
3) choice of crystal orientation for optimum detection sensi-
tivity (a feature noted in the Battelle experimental program).
The standard reference on the effects of crystal anisotropy in
cubic crystals (like YIG) is "Microwave Resonance Relations in
Anisotropic Single Crystal Ferrites,"[6] from which Figure 44

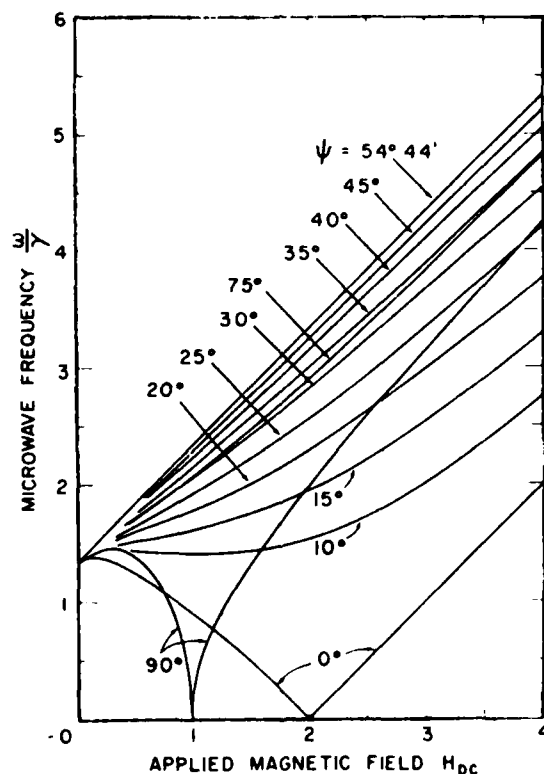Figure 44.   Ferromagnetic Resonance in Pure YIG as a Function
             of the Bias Field Angle ψ in the [110] Plane from
             the [100] Axis.   Vertical and horizontal scales
             normalized to $|K_1/M|$ (after Artman).

48

has been excerpted. This shows the variation of resonant frequency with applied magnetic field for various orientations of the field relative to the crystal lattice. The implications of field orientation on probe magnet design are obvious from these curves, where $\psi = 0^\circ$, 90°, and $54^\circ 44'$ refer to cases with the field along the [100], [110], and [111] directions, respectively. For pure YIG, $K_1/M = 80$ oe. Little information on the anisotropy field $2K_1/M$ is available for the gallium-doped YIG spheres used in our probes. A recent book, Magnetic Garnets,[7] does, however, give in Chapter 3 an overview of the effects of doping on magneto-crystalline anisotropy. From this it appears that gallium doping tends to reduce the anisotropy field. Other than this, all that can be done simply to compare the anisotropy field of doped YIG with the known value for pure YIG is to orient both samples along their easy directions in the same DC magnetic field and compare their resonant frequencies. It is known that the easy direction for gallium-doped YIG is the same as for pure YIG (i.e., [111]). When the magnetic bias field is applied along this direction, the magnitude of the field required for a particular resonant frequency is minimum. This choice of field orientation, therefore, minimizes the size of the samarium cobalt permanent magnet required in probe construction, an important factor in the case of bolt-hole probes.

In YIG filter technology ambient temperature compensation of the resonant frequency is of great engineering importance, and extensive work has been done on choosing the crystal orientation for this purpose. Unfortunately, there is no information in recent open literature giving details. For pure YIG it is known that temperature-compensated bias field directions lie along a cone of approximately 30° about the [100] axis. No information is available for the gallium-doped YIG used in our probes and the choice must be made experimentally, as is being done at Battelle following a variant of the procedures used in the YIG filter industry for orienting spheres.

A possible explanation of the observed crystal orientation dependence of probe sensitivity has been developed from theoretical work reported last year. The conclusion is that the flaw-liftoff signal ratio for a YIG probe should be larger for a DC magnetic field normal to the test piece surface than it is for a field parallel to the surface, as used in the current Battelle probes. This statement is based on a model of the YIG probe as an RF magnetic dipole rotating about the DC magnetic field in free space. When the probe is placed over a conducting test piece, the motion of the dipole is perturbed by the presence of its image in the conductor, so that the rotating dipole is elliptically (rather than circularly) polarized. An analysis of the liftoff effect according to this model was given in the Final Report of a previous contract.[3] An expression for the first

49

order liftoff signal for the YIG probe was given by Equation (B-19) in the previous Final Report. This is the signal that defines the liftoff axis (or I-channel signal) in a standard eddy scope presentation, where flaw detection is performed by observing the component of the flaw signal orthogonal to the I-channel axis. This orthogonal axis on the eddy scope presentation is defined as the Q-channel axis. In the Final Report it was shown that a second order liftoff signal determines the liftoff noise in the Q-channel and therefore establishes the flaw-liftoff signal-to-noise ratio in the Q-channel. The importance of this result is that the Q-channel flaw and liftoff signals both have the same frequency dependence for large a/δ, where the YIG probe operates, so that the YIG probe should theoretically have a somewhat better signal-to-noise ratio than a conventional coil operating at $a/\delta = 1$.

Although it was not found to analytically evaluate the second-order liftoff signal for the YIG probe, conclusions can be drawn from the form of the liftoff signal equation for an arbitrarily oriented dipole probe.[8] This showed that a vertical dipole has two times the liftoff sensitivity of a horizontal dipole, for both first- and second-order terms. In the same publication, it was shown that the horizontal dipole has 35% more flaw detection sensitivity than the vertical dipole, so that the horizontal dipole is theoretically predicted to have a flaw-liftoff signal-to-noise 2.7 times that of the vertical dipole. This full advantage is not expected to appear in the YIG probe, where [as shown in Equation (12) of the Final Report of a previous contract[3]] a crack-like flaw responds to only one component of the rotating RF dipole moment. However, a YIG probe with vertical DC bias field is still expected to have an advantage in flat-liftoff signal-to-noise over a horizontally biased probe. It should be noted that a vertically biased YIG probe can only function if the RF coupling coil is tilted with respect to the test piece surface, so that it provides an RF field component perpendicular to the DC field, or if a half-loop coupler is used.

One of the important goals of probe design is to choose a YIG sphere crystal orientation that optimizes sensitivity. It was seen above that the sensitivity depends on the direction of the axis about which the YIG dipole moment rotates. This discussion assumed that the dipole rotated about the axis of the DC magnetic field, i.e., magneto-crystalline anisotropy was neglected. In the presence of anisotropy, however, the dipole rotates about an axis determined by the strength of the DC magnetic field, and its orientation with respect to the crystal lattice of the YIG sphere.[6] Systematic optimization of the parameters of such a problem would be a very time-consuming task. However, it seems clear that the most likely optimum configura-

50

tion has the DC bias field normal to the test piece surface and the crystal oriented with its easy axis parallel to the DC field. In this case the magnetic dipole moment of the YIG rotates about the direction of the DC field, so that the flaw-liftoff signal-to-noise is maximum. Furthermore, the DC magnetic field required for operation is minimum, reducing the size of the permanent magnet required; and the YIG sphere is easily oriented in this way. This is obviously not consistent with the temperature compensation orientation described above, and probe design will have to be based on an engineering tradeoff between sensitivity, magnet size, temperature stability, and probe reproducibility.

3.2.5 Spin Wave Instabilities

Another aspect of YIG technology relevant to YIG probe design is the avoidance of nonlinear saturation effects due to spin wave instabilities. This subject is treated at length in Microwave Ferrites and Ferrimagnetics.[9] Generally speaking, as the excitation of the YIG resonance is increased the resonance response broadens and decreases in amplitude until it is barely visible. This effect is highly undesirable in devices, such as filters and EC probes, where proper functioning depends on having a strong sharp resonance. In these cases it is important to avoid operational parameters for which this saturation occurs at extremely low input power levels (on the order of microwatts). As explained in the Lax and Button reference (pp. 214-215), this depends entirely on the excitation frequency ω and the saturation magnetization $4\pi M_s$ of the YIG material. The condition required for avoiding this low level saturation is $f > 1.87$ $(4\pi M_s)$. For pure YIG $(4\pi M_s = 1750$ oe) f must be greater than 3270 MHz. For the $4\pi M_s = 250$ oe, to have better flaw characterization data, theory predicts that even lower frequencies should be desirable. This suggests that commercially available 125 oe material, which has a low frequency limit of 233 MHz, needs to be studied.

3.2.6 Responses to Fatigue Cracks, EDM Notches, and Scratches

In has been shown that probes operating at microwave frequencies are particularly sensitive to the opening of a flaw and are, therefore, readily able to distinguish between fatigue cracks and EDM notches or scratches and dents. The reason for this is the Faraday effect, i.e., a contribution to the flaw signal due to the magnetic flux of the probe field that enters the interior of the open flaw.[10] It is seen from the figure that the flaw opening term in the equation of ΔZ increases proportionally to frequency and tends to dominate the other terms at microwave frequencies. For this reason, a microwave probe has greater discrimination between a scratch and a fatigue crack (Figure 45) than does a probe operating in a megahertz frequency range.
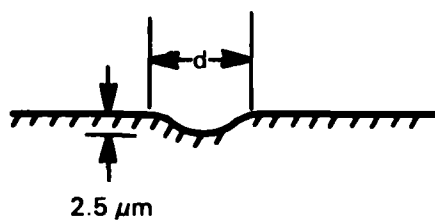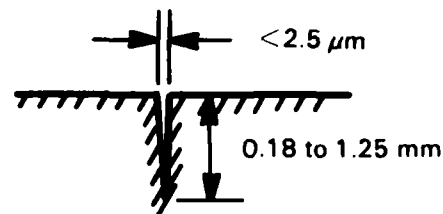
Scratch

d = 2.5 μm

Dent

d $\cong$ 0.25 to 2.5 mm

(a)   (b)

Figure 45.   Surface Flaws: (a) Scratch, (b) Fatigue Crack.

3.2.7   Parameter Optimization

    Scientific and technological factors entering into optimi-
zation of probe design parameters have been outlined in the
subsections above. As has been already noted, the requirements
are often contradictory and are further complicated by con-
siderations of probe fabrication. For example, the normal bias
field geometry recommended on the basis of maximum sensitivity
requires more difficult loop fabrication techniques and elimin-
ates the lateral shielding provided by the standard encircling
loop.   Strong coupling is also more difficult to achieve.
Engineering choices balancing these factors against practical
constraints in fabrication must be made to arrive at a satis-
factory probe design.

3.3   FEATURES OF THE FINAL EXPERIMENTAL DESIGN

    Figure 46 shows the essential features of the Battelle
rotary probe design, described in detail in the experimental
part of this report. The single coupling loop and the YIG sphere
are mounted at the end of the probe shaft, which contains the
miniaturized electronics, and a coaxially mounted permanent
magnet is mounted on the other side of the YIG sphere. It is very
important to have the magnet attached rigidly to the sphere
mount. The field of a small magnet, suitable for insertion into
a bolt hole, is nonuniform and motion of the magnet relative to
the sphere produces large changes in the oscillator frequency
and amplitude.   This complicates the adjustment of magnetic
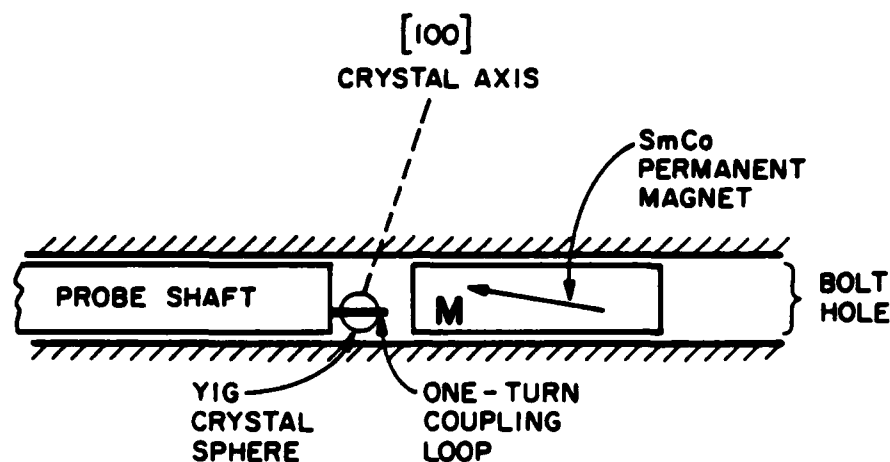field direction described in the previous section.   In the

52

Figure 46. Schematic of Miniaturized Ferromagnetic Resonance
   Probe.

Battelle design this adjustment is accomplished by cutting the
permanent magnet with the permanent magnetization skewed rela-
tive to the axis of the hole. By rotating the magnet assembly
about the hole axis, one can change the magnetic field direction
relative to the YIG sphere. In assembling the probe the YIG
sphere is mounted on an insulating shaft and held in the coupling
loop. The sphere and magnetic field orientations can then be
adjusted in air, to give satisfactory oscillator operation.

It was noted in the previous section that careful choice of
the crystal and magnetic field directions is required to achieve
good flaw-liftoff signal separation. With the small magnet
shown in Figure 46 this is complicated by the fact that the
magnetic field diverges from the ends of the magnet and is quite
nonuniform at the position of the YIG sphere. This nonuniformity
of the DC bias field applied to the sphere has a direct effect
on the flaw-liftoff separation. Furthermore, the mean value of
the magnetic field at the sphere, as well as its direction,
depend on the spacing between the magnet and the sphere. In
addition, the rotational adjustment of the magnet, described
above, can only move the magnetization in a cone about the axis
of the probe. For these reasons, setting the magnetic field
direction is limited to certain orientations. In the experi-
mental part of the program, flaw-liftoff separation has not been
achieved in the geometry of Figure 46, even though it was
successfully demonstrated on the nonminiaturized probe struc-
ture during the first year of this contract. Suggested further
strategies for achieving separation include adjusting the probe
in air for separation, with a relatively uniform dc magnetic
field and a plane metal surface, setting up the same orientations
in the geometry of Figure 46, and then fine tuning in the final

53

bolt hole geometry. To improve the flexibility of the fine tuning it would be desirable to have more complete control of the magnetic field direction, which is restricted to a conical path by the magnet geometry of Figure 46. This might be realized by an adjustable soft iron shunt around the permanent magnet.

Two features of probe design relative to the YIG sphere itself were described in subsections 3.2.4 and 3.2.5 of the previous section. The first concerns temperature compensation, which requires a suitable choice of orientation of the crystal sphere. This criterion is in conflict with the flaw-liftoff separation optimization described above, and it is not clear at this stage that a satisfactory compromise can be achieved. In an eddy current probe long term temperature stability is not as important as it is in a YIG filter and no attempt has been made to achieve this compromise in the final probe design, although temperature effects were investigated experimentally at Battelle. Subsection 3.2.5 dealt with nonlinear saturation effects. These were observed experimentally but do not constitute a limitation. Noise in an eddy current detector is dominated by liftoff and tilt, which vary with the oscillation amplitude in the same way as the flaw signal itself. There is, consequently, no need to increase the oscillation level to the point where saturation effects occur, at least for the high level saturation effects described in <u>Microwave Ferrites and Ferrimagnetics</u>.[9] Care must be taken, however, to avoid the low level saturation effects described in subsection 3.2.5. As was stated, this effect can be eliminated by suitably selecting the saturization magnetization of the YIG. This is the reason for choosing YIG spheres with a $4\pi M_S$ of 250 oersteds in the current probes, which permits operation down to approximately 500 MHz. For improved flaw characterization it would be desirable to operate at even lower frequencies, and experiments were performed at Battelle on 150 oersted material. However, it was not found possible to achieve satisfactory coupling with a single turn loop in this material. Two turn loops may solve this problem, but at the cost of more difficult fabrication and increased probe size.

It was pointed out in subsection 3.2.6 of the previous section that microwave frequency probes are much more sensitive to open flaws than are probes operating in the megahertz frequency range. For this reason, it is important to perform tests on real fatigue cracks as well as on EDM notches. In the experimental part of this report results are given for compact ferromagnetic resonance probes without flaw-liftoff separations, and it can be seen that liftoff is not a serious problem. Figure 47 shows some results obtained with a passive ferromagnetic resonance (FMR) probe under a previous program at Stanford. This demonstrates that, despite the shortcomings of the passive probe, fatigue cracks with lengths as small as 140 μm and spacings on the order
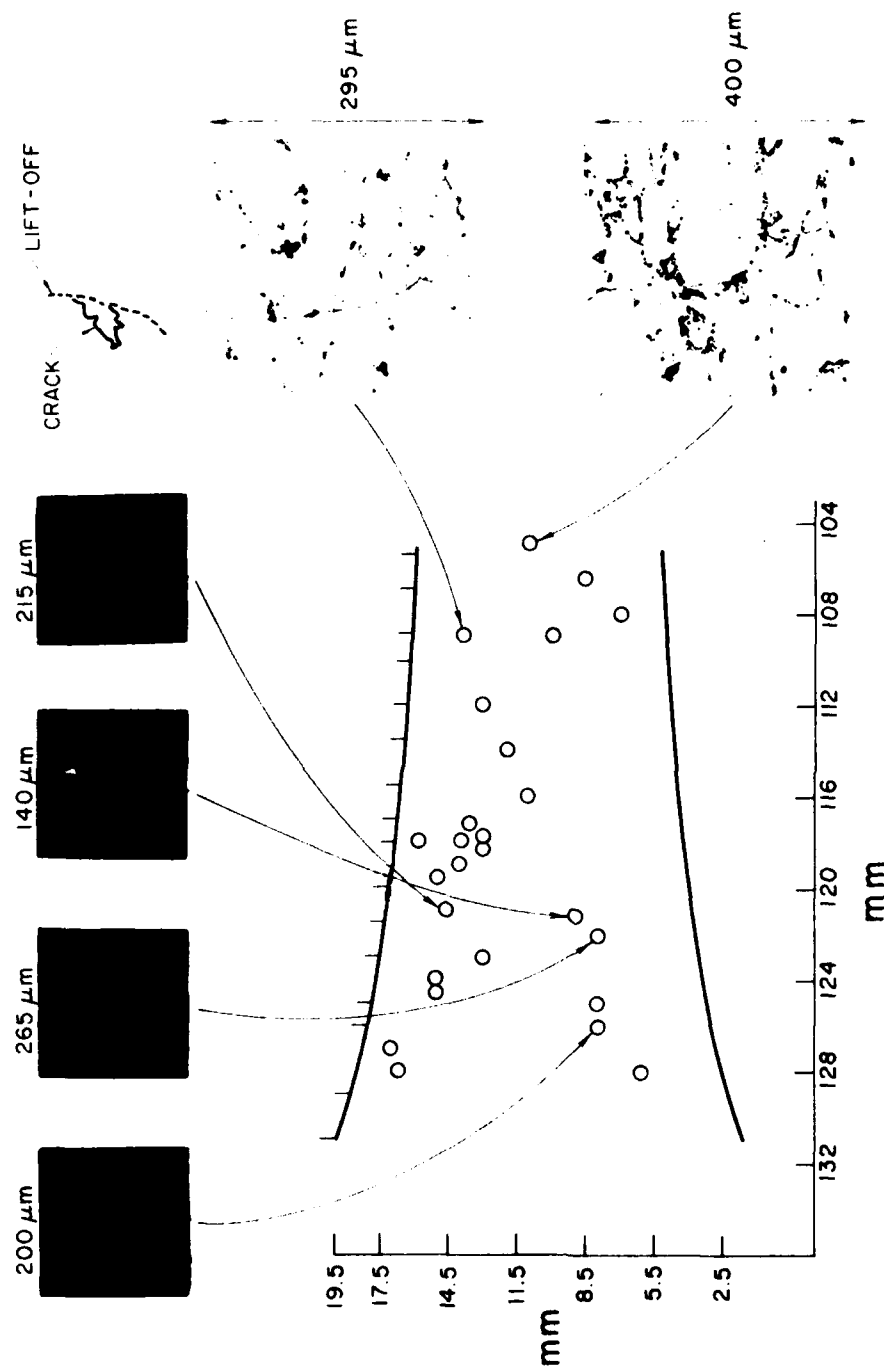
Figure 47. FMR EC Signals from a Cluster of Fatigue Cracks in AL 2219-T851.

of a millimeter can be resolved. Comparative tests with conventional probes were unable to detect these flaws. The strong liftoff line curvature in passive FMR probes was a major disadvantage of this experiment, as it limited the amount of Q-channel gain that could be used. In spite of this, very good signal-to-noise has been achieved. Detection with equal, or greater, sensitivity is to be expected in an active probe adjusted for flaw-liftoff separation.

3.4 COMPARISON OF MICROWAVE FMR AND CONVENTIONAL MEGAHERTZ FREQUENCY PROBES

If the criterion of detection sensitivity is taken to be the ratio of flaw signal to liftoff signal in the Q-channel, the highest sensitivity for a closed surface breaking crack of depth a is reached when $a/\delta > 1$.[8] For a = 0.175 mm in a material such as IN-100 or titanium, this point occurs at approximately 8 MHz. In the region between $a/\delta = 1$ and 10, i.e., between 8 and 800 MHz, the sensitivity increases slightly and eventually saturates. An 800 MHz probe is therefore not expected to have much greater sensitivity for a 0.175 mm closed crack than does an 8 MHz probe. (For an open flaw, the high frequency probe is expected to have a significantly greater sensitivity.)

The FMR probe does, however, have a number of important advantages. First, the electrical structure is very easy to fabricate. It requires only a single-turn loop and can be made with a very small diameter. (At the present time, only spheres down to 0.3 mm in diameter are available commercially, but this does not appear to be a limitation to the fabrication process.) It has been shown experimentally at Battelle that the coupling loop screens the probe field, so that shielded probe operation is obtained with a very simple structure. The FMR probe also has enhanced discrimination against scratches, which are widely opened flaws (Figure 45). Because of the Faraday effect described above, the phase angle of the flaw signal differs greatly from that of a crack at high frequencies.

The ferromagnetic resonance probe has also been shown in earlier work at Stanford to function well on magnetic work pieces, provided the magnet structure is correctly designed. At microwave frequencies magnetic metals have very high losses and detection is not due to eddy currents, but to a perturbation of the DC bias field by the flaw in the magnetic work piece. To operate over a magnetic work-piece, the FMR probe must have its bias field normal to the surface (Figure 48). The magnetic work-piece acts as part of the magnetic return path, rather than "shorting out" the magnetic field applied to the sphere. When the probe passes over a flaw, the DC magnetic field pattern shifts, as shown in the figure, and changes the frequency and
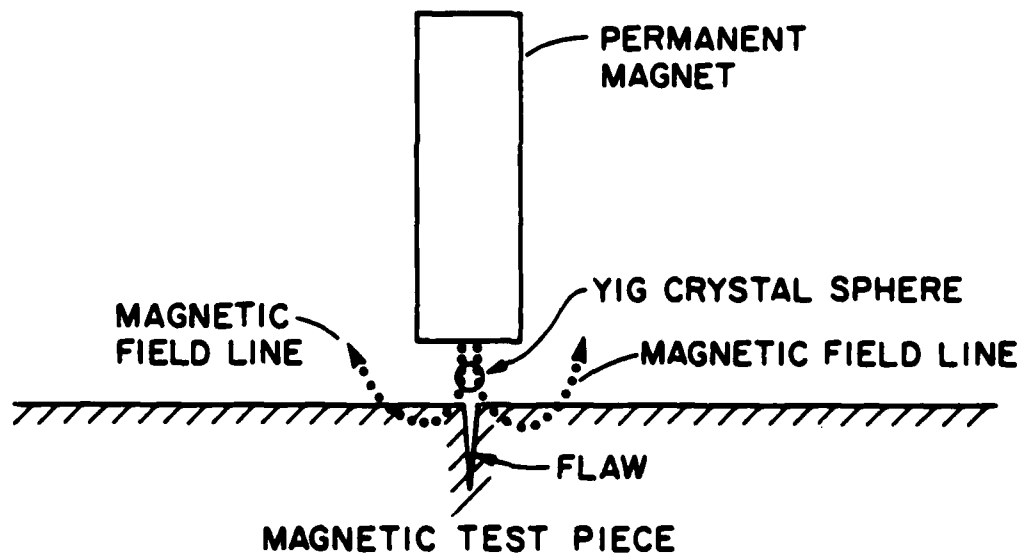
56

Figure 48. FMR Probe Detection of Surface Cracks in Magnetic
Work Pieces.

amplitude of the oscillation. In this application the probe
operates in the manner of a magnetic particle detector, in which
small magnetic particles are used to detect magnetic flux
leakage around cracks in a magnetic work-piece that is mag-
netized by an external electormagnet. The advantage of the FMR
"magnet particle detector" is that it is small and portable,
since magnetization of the component under test is required only
near the crack.

57

4.0 SUMMARY AND CONCLUSIONS

Experiments were performed that provided data for the characterization of the FMR probe in both the passive and active modes of operation. The thrust of this characterization effort was to determine the limitations of the FMR-MEC technique as a function of probe liftoff, specimen material, and specimen and flaw geometries. Several active probe designs were evaluated including one for a dual-differential probe. Major advancements were made in the active probe signal processing circuitry that have provided flaw/liftoff discrimination from a single probe. The new signal processing method provides liftoff noise suppression with the single probe.

Battelle and Stanford also studied the effects of the physical constraints involved in a probe design for inspection in a jet engine interstage seal key slot geometry. Specifically, the key slot inspection requires that the probe access a geometry equivalent to a 3.5 mm diameter hole. This resulted in major advancements in the miniaturization of the active FMR probe as well as in the development of enhanced fabrication techniques.

Based on these laboratory experiments and theoretical studies, a rotary probe inspection system was developed for inspecting small radius curve surface as well as flat surface geometries. The experimental results achieved with the rotary probe demonstrate that the extremely high operating frequency of the active FMR eddy current probe does not limit its effectiveness for crack detection in conditions of widely varying liftoff. This system also demonstrated that the active FMR probe and signal processor circuitry can be made practical, simple, and compact. In particular, we feel that one of the primary advantages of the active FMR probe over conventional coil probes is its extremely small effective eddy current field diameter (or crack detection resolution) which is 0.38 mm utilizing a 0.30 mm YIG. This is important for sizing cracks in tight geometries. With the use of hybrid integrated circuit fabrication techniques, it should be possible to reduce the diameter of the small radius active FMR probe to inspect even tighter geometries such as 3.13 mm diameter cooling holes with an effective eddy current field resolution of less than 0.38 mm.

REFERENCES

1. P. M. Ollivier, "Microwave YIG-Tuned Transistor Oscillator Amplifier Design: Application to C Band," *IEEE J. Solid-State Circuits* SC-7 54-60, February 1972.

2. J. C. Papp and Y. Y. Koyano, "An 8-18 GHz Tuned FET Oscillator," *IEEE Trans*. MTT-28 762-767, July 1980.

3. J. M. Prince and B. A. Auld, "Research to Develop and Evaluate Advanced Eddy Current Sources for Detecting Small Flaws in Metallic Aerospace Components," Battelle, Pacific Northwest Laboratories, Final Technical Report, AFWAL-TR-82-4145, December 1982.

4. B. A. Auld, "Theoretical Characterization and Comparison of Resonant Probe Microwave Eddy Current Testing with Low Frequency Eddy Current Methods," in *Eddy Current Characterization of Materials and Structures*, G. Birnbaum and G. Free, Eds., Philadelphia: ASTM STP 722, 1981.

5. B. A. Auld and D. K. Winslow, "Microwave Eddy Current Experiments with Ferromagnetic Resonance Probes," ibid, pp. 348-366.

6. J. O. Artman, "Microwave Resonance Relations in Anisotropic Single Crystal Ferrites," *Proc. IRE*, 44, pp. 1284-1293, 1956.

7. G. Winkler, *Magnetic Garnets*, F. Wieweg and Son, Braunschweig/Wiesbaden.

8. M. Riaziat and B. A. Auld, "Eddy Current Probe Design and Matched Filtering for Optimum Flaw Detection," *Review of Progress in Quantitative NDE*, Vol. 2, D. O. Thompson and D. E. Chimenti, Eds., pp. 189-204, 1983.

9. B. Lax and K. J. Button, *Microwave Ferrites and Merrimagnetics*, pp. 206-227, McGraw-Hill, 1962.

10. B. A. Auld, F. Muennemann, M. Riaziat, and D. K. Winslow, "Analytic Methods in Eddy Current NDE," *Review of Progress in Quantitative NDE*, Vol. 1, D. O. Thompson and D. E. Chimenti, Eds., pp. 363-367, 1982.

END

FILMED

9-85

DTIC